ACS OMEGA

http://pubs.acs.org/journal/acsodf

Article

D-Glucose Oxidation by Cold Atmospheric Plasma-Induced Reactive Species

Mohsen Ahmadi,* Zahra Nasri, Thomas von Woedtke, and Kristian Wende*

Cite This: *ACS Omega* 2022, 7, 31983−31998

Read Online

ACCESS | Metrics & More | Article Recommendations | Supporting Information

ABSTRACT: The glucose oxidation cascade is fascinating; although oxidation products have high economic value, they can manipulate the biological activity through posttranslational modification such as glycosylation of proteins, lipids, and nucleic acids. The concept of this work is based on the ability of reactive species induced by cold atmospheric plasma (CAP) in aqueous liquids and the corresponding gas−liquid interface to oxidize biomolecules under ambient conditions. Here, we report the oxidation of glucose by an argon-based dielectric barrier discharge plasma jet (kINPen) with a special emphasis on examining the reaction pathway to pinpoint the most prominent reactive species engaged in the observed oxidative transformation. Employing D-glucose and D-glucose-$^{13}C_6$ solutions and high-resolution mass spectrometry and ESI-tandem MS/MS spectrometry techniques, the occurrence of glucose oxidation products, for example, aldonic acids and aldaric acids, glucono- and glucaro-lactones, as well as less abundant sugar acids including ribonic acid, arabinuronic acid, oxoadipic acid, 3-deoxy-ribose, glutaconic acid, and glucic acid were surveyed. The findings provide deep insights into CAP chemistry, reflecting a switch of reactive species generation with the feed gas modulation (Ar or Ar/O_2 with N_2 curtain gas). Depending on the gas phase composition, a combination of oxygen-derived short-lived hydroxyl ($^{\bullet}$OH)/atomic oxygen [O(^{3}P)] radicals was found responsible for the glucose oxidation cascade. The results further illustrate that the presence of carbohydrates in cell culture media, gel formulations (agar), or other liquid targets (juices) modulate the availability of CAP-generated species *in vitro*. In addition, a glycocalyx is attached to many mammalian proteins, which is essential for the respective physiologic role. It might be questioned if its oxidation plays a role in CAP activity.

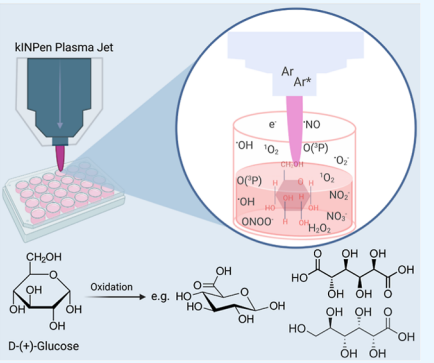

INTRODUCTION

Cold atmospheric plasma (CAP), as an emerging technology, was found effective in a wide range of biomedical and biotechnical applications such as chronic wound care,[1−3] implant optimization,[4] cancer therapy,[5,6] food processing,[7,8] nanotechnology, and catalytic materials.[9] Plasma sources can adopt a wide range of designs[10,11] yet for clinical and biomedical research plasma jets such as the kINPen dominate.[12] To current knowledge, the interference of CAP-derived reactive oxygen and nitrogen species with cellular redox signaling processes triggers diverse downstream events on the biological level.[13,14] Among these, modulation of immune responses and changes in cell survival stand out. Determined by the individual design of a CAPs source and controlled by parameter variation, various short- and long-lived reactive species such as singlet oxygen ($^1O_2$), hydroxyl radical ($^{\bullet}$OH), atomic oxygen [O(^{3}P)], superoxide anion radicals ($^{\bullet}O_2^-$), ozone (O_3), nitric oxides (N_xO_y), and hydrogen peroxide (H_2O_2) are generated alongside free electrons, and neutral particles (e.g., metastable argon (Ar), Ar*, Ar_2, and N_2).[12,15−18] In addition, auxiliary effects of (vacuum-) UV radiation and electromagnetic fields are discussed.[19,20]

While electrical fields and long-lived species have a significant penetration depth, UV radiation and the primary short-lived species are confined to the surface. It is assumed that they contribute to the effect of the chemical impact on the target molecules, especially proteins.[21−24]

In contrast, the chemical impact of CAP on carbohydrates remains underexplored so far, with only a few reports available. Li *et al.*[25] reported that treating 20 mM of aqueous (D_2O/PBS) sugar solutions (D-ribose, D-glucose, and D-sucrose) with air dielectric-barrier discharge plasma (1 mm distance of contact surface) led to a full decomposition into low-molecular-weight organic acids, for example, oxalic, glycolic, tartaric, glyceric, and formic acid. However, in the majority of *in vitro* studies investigating CAP effects, carbohydrates are involved as the primary energy source of cell culture media (5−10 mM) or as gelling agents (% range).[6,26] The potential oxidation products may contribute to the observed effects and the subsequent conclusions.

Received: May 12, 2022
Accepted: August 16, 2022
Published: August 26, 2022

Besides fundamental considerations in CAP-related biomedical research, the oxidation of carbohydrates by CAP as a scalable and cost-efficient method may offer new opportunities in chemical processing. An increasing interest in carbohydrate conversion into high-value compounds utilized as food additives, detergents, antioxidants, cosmetics, biodegradable polymers, pharmaceutics, and medicinal products[27] led to the development of various (bio)catalytic methods besides the traditional chemical oxidation,[28] for example, enzymatic oxidation,[29] nanoparticle-based electrolysis,[30] metal nanozymes,[31] supported transition metal-catalyzed oxidation,[32,33] and electrochemical oxidation.[34] The depolymerization of biomass (75% carbohydrates) for glucose fuel cells or to produce valuable chemicals, such as aldonic acids and aldaric acids, lactones, gluconolactone, glucarolactones, and other sugar acids, are another focus.[35−37]

It is reported that the hydroxyl radical plays the main role in glucose oxidation, for example, in catalyst-free ultrasonic irradiation,[38] photocatalytic transformation,[39] heat sterilization,[40] and microwave reactions.[41] Taking this existing knowledge on the mechanism of reactive species−based glucose oxidation modifications into account, we intended to shed more light on the D-glucose oxidation cascade by CAP-induced reactive species. The argon jet plasma applied for the study delivers $^{\bullet}OH$ and O_2^- radicals along with singlet oxygen $O_2(^1\Delta_g)$ and atomic oxygen $O(^3P)$ radicals, ultimately yielding H_2O_2 as long-lived reactive species.[42−44]

Since glucose is an isomeric molecule with several chiral carbons and a high possibility of oxidation and polymerization, the structure elucidation of glucose oxidation products is challenging. However, a deep understanding of the CAP oxidation mechanism and the role of engaged reactive species is required. To achieve this, a combination of electrospray ionization high-resolution mass spectrometry and tandem MS/MS spectrometry was employed, taking recently published approaches into account.[45,46] In addition, we used isotopic labeling (D-glucose-$^{12}C_6$ and D-glucose-$^{13}C_6$) to infer the origin of the oxidation products. Besides the CAP-focused knowledge gain, we explored the opportunity of utilizing CAP-induced reactive species to oxidize glucose concerning carbohydrate oxidation chemistry and low-MW carbonomics.

METHODS AND PROCEDURES

Sample Preparation. The 50 mM stock aqueous solution of D-glucose and D-glucose-$^{13}C_6$ (Sigma-Aldrich) was prepared. The glucose solution was diluted in H_2O to a final concentration of 2 mM before each treatment experiment. In the setup, the gas flux-mediated evaporation was compensated by adding the predetermined amount of H_2O to keep the initial concentration constant. All treated samples with the denoted gas variations from 1 to 10 min were divided into aliquots and diluted in a 1:4 ratio (v/v) using 20% methanol (MeOH) in 5 mM of ammonium formate (Sigma-Aldrich Chemie GmbH, Germany) solution at pH 7.4 in order to be subject to the high-resolution mass spectrometry. Mass spectroscopy experiments were performed for plasma treatment time points (1, 5, and 10 min), and resulting D-glucose oxidation modifications were assessed. All samples were incubated for 2 h before subjecting to the mass spectrometer at ambient temperature.

Cold Atmospheric Plasma Treatments. All experiments were performed at ambient temperature using a kINPen IND (kINPen; neoplas tools GmbH, Germany). The argon (Ar) gas flow rate was set at 1.5 and 3 standard liters per minute (slm) of pure argon that served as the main feed gas. The cold plasma is generated at the tip of the central electrode and expands into the ambient air. For some experiments, the plasma effluent was shielded by a N_2 curtain (3 slm) to avoid interfering with atmospheric oxygen. Plasma treatment was performed in four regimes: 3 slm Ar, 3 slm Ar/0.5% O_2, 1.5 slm Ar + N_2 curtain gas, and 1.5 slm Ar/0.5% O_2 + N_2 curtain gas. 3 slm N_2 curtain gas was applied. All gases were purchased from Air Liquide, France (99.999% pure). A 750 μL volume of aqueous glucose solution (2 mM) was placed in a 24 well-plate (Sarstedt, Germany) and treated from 1 to 10 min with a plasma jet nozzle to a liquid distance of 9 mm for all plasma treatments. A tiny chamber equipped with a borofloat-33 window (25 mm × 1 mm, Nano Quarz Wafer GmbH) and MgF_2 window (25 mm × 1 mm, Korth Kristalle GmbH) were employed to determine the role of vacuum ultraviolet (VUV)/ultraviolet radiation (UV) irradiation by blocking the gas−liquid interface as reported.[19]

Mass Spectrometry Analysis. To elucidate the D-glucose ($^{12}C/^{13}C$) oxidation products, high-resolution mass spectrometry was performed using a TripleTOF 5600 mass spectrometer from AB Sciex. All 400 μM diluted samples in 20% MeOH in 5 mM of ammonium formate were directly infused (7 μL/min) into the turbo ion source using negative electrospray ionization. Survey spectra acquisition was performed in a range of 20−1000 (m/z), and peaks were fragmented using collision-induced dissociation. The MS system was calibrated using Sciex tuning solution containing cesium iodide. All samples were subjected to using identical system settings (capillary temperature: 250 °C), curtain gas: 35 psi N_2, ion source gas 2: 35 psi N_2, and ion spray voltage: 3.8 kV. Oxidation product fragmentation spectra (MS/MS) were acquired in the product ion mode (collision energies: 10−70 eV and declustering potential: 80 V). All spectra were normalized, peak areas were calculated, and duplicates with standard deviation were shown.

Reactive Oxygen Species Assays and Liquid Analysis. Singlet oxygen [$^1O_2(a^1\Delta_g)$] was determined using a singlet oxygen sensor green (SOSG, Invitrogen from Thermo Fisher, USA), and its fluorescence was measured at $\lambda_{ex}/\lambda_{em}$ 485/535 nm.[24] Hydrogen peroxide (H_2O_2) was quantified *via* its reaction with titanium(IV) oxysulfate ($TiOSO_4$, 5% Ti(IV) in sulfuric acid, Sigma-Aldrich Chemie GmbH, Germany) according to previous protocols,[47] and measured at λ_{ex} 407 nm. In some experiments, H_2O_2 was analyzed using the Amplex UltraRed reagent stock (Invitrogen, USA) according to the reported protocols.[48] OH/O radicals were analyzed by terephthalic acid (TPA) assay.[49] 5 mM TPA was treated with plasma, and the fluorescence of the product 2-hydroxyterephtalic acid (HTPA) was measured at $\lambda_{ex}/\lambda_{em}$ 360/465 nm. All aforementioned samples were analyzed using a Tecan plate reader (infinite M200 pro, Tecan Group Ltd., Switzerland). An electrochemical sensor was employed for the measurement of CAP-generated hypochlorite produced *via* the reaction of atomic oxygen [$O(^3P)$] with chlorine in phosphate-buffered saline (PBS). The sensor consisted of a toluidine blue redox system covalently attached to a gold electrode, which can precisely detect hypochlorite in solution.[50] A calibration curve was plotted based on the current-time response of the sensor recorded by a potentiostat AUTOLAB PGSTAT302N (Deutsche METROHM GmbH & Co. KG, Germany) in PBS (pH 7.4) at 0.30 V versus Ag/AgCl reference electrode for

https://doi.org/10.1021/acsomega.2c02965
ACS Omega 2022, 7, 31983−31998

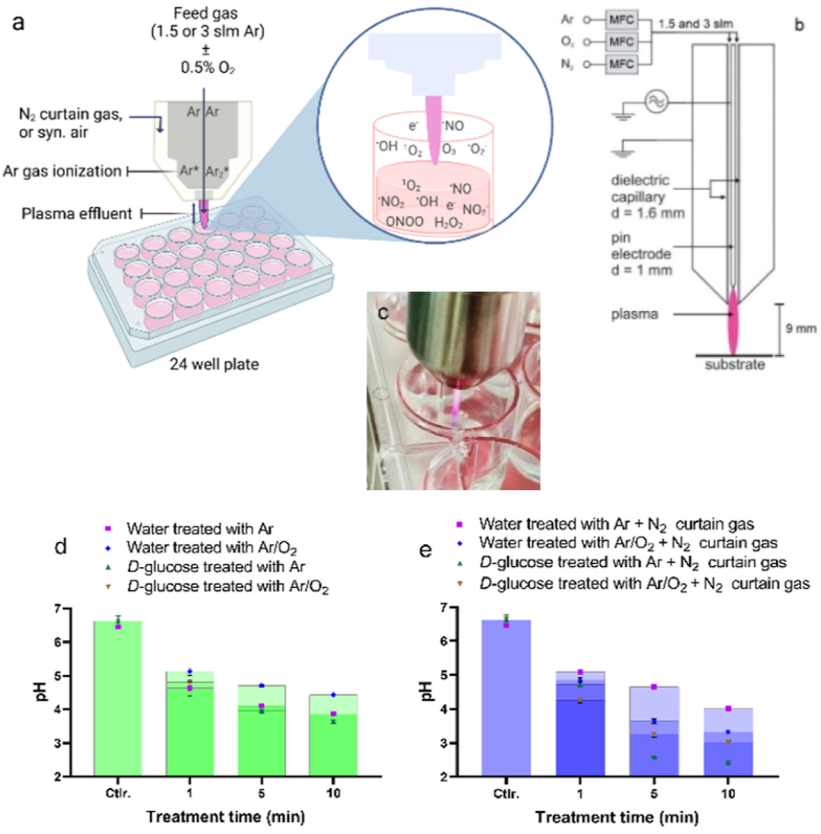

Figure 1. (a) Schematic illustration for the plasma treatment of 750 μL D-glucose solution in a 24 well plate (the nozzle of the kINPen device could be shielded with N_2 flow that affects the type of reactive species production), (b) schematics of the kINPen IND plasma jet (reprinted with some minor changes with permission from ref 55 (Lackmann *et al.*[55]), Copyright 2018, Springer Nature, http://creativecommons.org/licenses/by/4.0/); (c) plasma jet and its effluent applied to treat D-glucose solutions; (d) pH of the water and D-glucose solution measured after plasma treatment with Ar and Ar/O_2 admixture regime; (e) pH of the water and D-glucose solution measured after the same plasma treatment regime with only the nozzle shielded with the N_2 flow. MFC = mass flow controller and slm = standard liter per minute.

successive addition of hypochlorite. Then, the plasma-treated samples were analyzed at the same potential. The quantification of nitrite (NO_2^-)/nitrate (NO_3^-) was performed *via* ion chromatography (ICS-6000, Thermo Fisher Scientific), according to a protocol reported by Lackmann *et al.*[51] Each treatment condition was triplicated for each assay.

Data Analysis and Visualization. Data acquisition, mass signal integration, and calculation were performed by using Analyst TF 1.51 software (AB Sciex), Peakview software (version 1.1.1.2, AB Sciex), and Prism 9 (version 9.2.0, GraphPad Software, USA). Data are from two independent experiments (each with technical duplicates) and show mean and standard deviation.

RESULTS AND DISCUSSION

Cold Atmospheric Plasma Treatment. In this study, oxidation of glucose was carried out using a kINPen argon plasma jet. The kINPen consists of a grounded ring electrode enclosing a ceramic capillary having a 1.6 mm diameter, where a powered central rod electrode is located inside (2−6 kVpp at 1.1 MHz). The Ar gas flow was kept constant inside the capillary and admixed with O_2 as the second feed gas, as shown in Figure 1a,b. In addition, N_2 curtain gas was also applied in parallel to exclude atmosphere gasses that impact the CAP-induced reactive species chemistry (Figure 1a). The N_2 curtain gas shielded the active effluent and protected the reactive species from colliding with ambient molecular oxygen. Thereby, the type and concentration of sensitive, reactive species, especially atomic oxygen, increases and allows interaction with the liquid and entities dissolved in the solution.[52] Our previously published investigations well shown the influence of several parameters, for example, gas composition and flow rate, the distance of nozzle jet to solution surface, and exposure duration of samples to the reactive species.[53] These parameters directly impact the concentration and type of generated reactive species, which will be discussed in the subsequent section.

In the first step, 2 mM D-glucose in pure water was exposed to CAP (Figure 1c), and the pH of pure water and D-glucose solutions was monitored (Figure 1d,e). The pH dropped significantly with treatment time, especially in the D-glucose solution samples, which are associated with the significant production of acids. After 5 min of plasma treatment under Ar and Ar/O_2 + N_2 curtain gas, the pH values dropped to below 3.5. Further treatment up to 10 min yielded a minimum pH value of 2.5. The pH of the solution after Ar plasma treatment was more acidic than in the Ar/O_2 case, reflecting the different formations of nitric acid and nitrous acid during the plasma treatment.[54] Notably, a contribution of produced acids by CAP in D-glucose-containing samples must be considered.

D-Glucose Oxidation Products. The mass spectra of diluted samples of D-glucose, D-glucose-$^{13}C_6$, and 1:1 (v/v) ratio of D-glucose and D-glucose-$^{13}C_6$ were recorded after plasma treatment. This dilution was considered to improve the

https://doi.org/10.1021/acsomega.2c02965
ACS Omega 2022, 7, 31983−31998

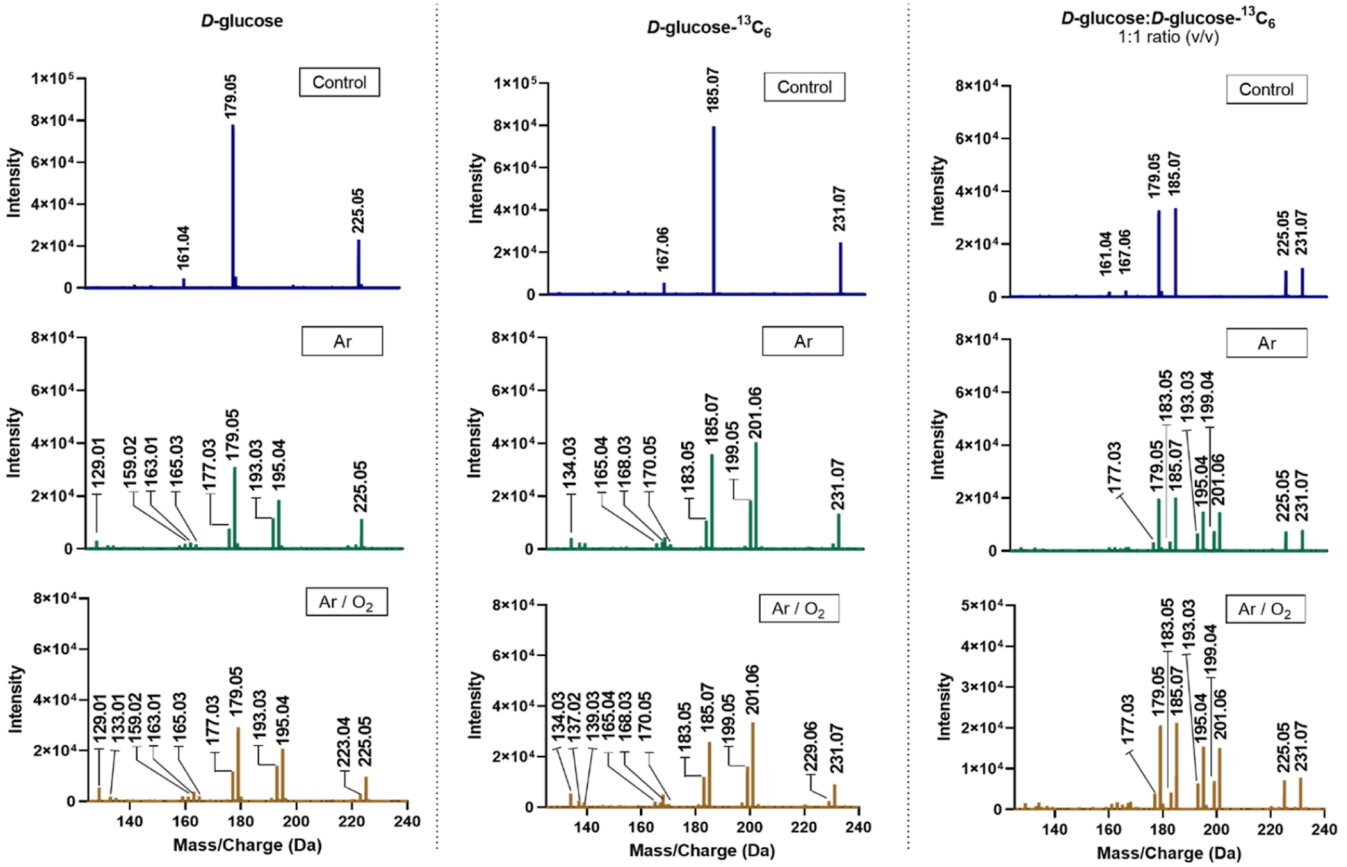

Figure 2. High-resolution mass spectra included ^{12}C and ^{13}C atoms after plasma treatment with the denoted gas variations for 10 min. (Left) Mass spectra of D-glucose, (Middle) mass spectra of D-glucose-$^{13}C_6$, and (Right) mass spectra of a 1:1 ratio (v/v) of D-glucose and D-glucose-$^{13}C_6$. The applied plasma gas variations are shown with surrounded box (see Method and Procedures section for more details).

signal intensity of glucose oxidation products by forming the anionic adducts.[45] The D-glucose-$^{13}C_6$ solutions were examined to elucidate the oxidative modifications (and fragmentation pattern) regarding the multiple oxidations pathways. In addition, a mixture of D-glucose and D-glucose-$^{13}C_6$ solutions was treated to clarify the possible reaction of carbon dioxide from the air with CAP-induced ROS and its effect on the abundance of glucose oxidation products.

The mass spectra of D-glucose solutions after plasma treatment for 10 min versus untreated sample are shown in Figure 2. Full-range mass spectra (20−1000 *m/z*) of all aforementioned samples before and after plasma treatment are collected in Supporting Information (Figures S1−S13). As shown in Figure 2, the MS signal for D-glucose was observed at *m/z* 179.05 $[C_6H_{12}O_6-H]^-$, whereas unit charged ion at *m/z* 185.07 belongs to the D-glucose-$^{13}C_6$ with 6 amu higher weight due to the ^{13}C atoms. In addition, the D-glucose can be seen by the $[C_6H_{12}O_6 + CHOO]^-$ at *m/z* 225.05 (monoisotopic mass of formate is 44.9982), whereas the D-glucose-$^{13}C_6$ was observed at *m/z* 231.07. The MS signal at *m/z* 178.03 might belong to the concurrent formation of a $[C_6H_{12}O_6-2H]^{-\bullet}$ radical anion.[56] The signal at *m/z* 161.04 (167.06 *m/z* for D-glucose-$^{13}C_6$) is formed by the loss of one water molecule $\{[C_6H_{10}O_5-H]^-\}$ and a double bond formation (Figure 2).

Additionally, other fragment anions were observed at *m/z* 359.11, 367.09, 381.09, and 547.15 (Supporting Information Figure S2). The MS signals at *m/z* 359.11 (MS/MS fragmentation: *m/z* 359.11 → 179.04, 161.03, 119.02, and 89.01) are derived from a noncovalent glucose−glucose complex in the negative ion mode $\{[C_{12}H_{24}O_{12}-H]^-\}$, most likely due to its high intermolecular hydrogen bonds.[45,57] The corresponding ions were also observed in the mass spectra of D-glucose-$^{13}C_6$ samples at *m/z* 371.15. However, the ESI-MS/MS of other observed signals, as shown in Figure S2, are most likely derived from the dissociation of deprotonated glucose, and the deprotonated ion can undergo oligomerization.

Delaux *et al.*[58] reported that generated radicals in the gas phase of the nonthermal atmospheric plasma could reasonably react with cellulose, cleaving the glycosidic bonds and yielding soluble oligomers. However, further oxidation of carbohydrates by CAP-induced reactive species has not been studied to the best of our knowledge. The postulated reaction mechanism of D-glucose oxidation is depicted in Scheme 1 based on the finding of our experiments and published studies on catalyst-driven glucose oxidation.[30,33,59] The number of MS signals increased significantly after plasma treatment, corresponding to various products evolved from alcohol (−OH) oxidation to predominantly form aldehydes (−CHO) and carboxylic acids (−COOH). The primary oxidation products of both D-glucose and D-glucose-$^{13}C_6$ yielded from CAP-induced reactive species are listed in Table 1. The structures of the different D-glucose oxidation modifications were also examined by ESI-MS/MS analysis and respective fine masses (see Table 1 for both D-glucose and D-glucose-$^{13}C_6$).

The products at *m/z* 195.04, 193.03, and 177.03 were more predominant, as shown in Figure 1. The D-gluconic acid $[C_6H_{12}O_7-H]^-$, 195.04 *m/z* is the most abundant oxidation product. As shown in Table 1, the MS/MS spectrum of the

https://doi.org/10.1021/acsomega.2c02965
ACS Omega 2022, 7, 31983−31998

Scheme 1. Postulated Oxidation Modifications of D-Glucose after Plasma Treatment[30,33,59a]

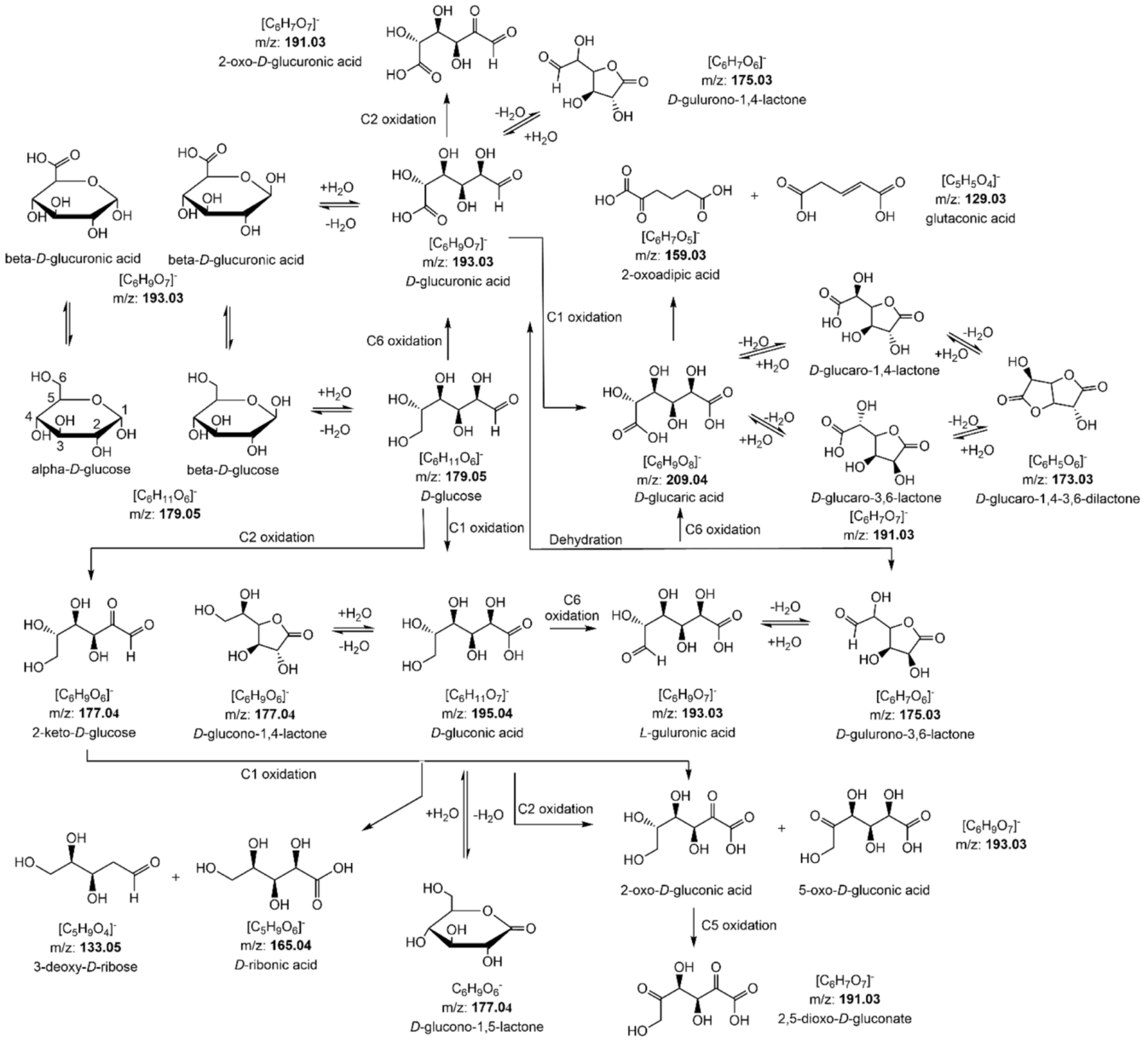

[a]Partially adopted with permission from ref 30 (Copyright 2020, Springer Nature, https://creativecommons.org/licenses/by/4.0/), ref 33 (Copyright 2019, American Chemical Society (ACS), https://creativecommons.org/licenses/by/3.0/)., and ref 59 (Copyright 2020, Royal Society of Chemistry (RSC), https://creativecommons.org/licenses/by-nc/3.0/).

signal at *m/z* 195.04 is comparable with commercially available D-gluconic acid in the same infusion method (MS/MS 195.05 → 129.01, 75.00, and 59.01, see Supporting Information Figure S15).

The D-gluconic acid can be oxidized further, yielding, for example, $[C_6H_{10}O_7{-}H]^-$ (193.05 *m/z*) and $[C_6H_{10}O_6{-}H]^-$ (177.03 *m/z*) in different pathways (Scheme 1). The oxidation of the aldehyde (−CHO) group of glucose to produce the gluconic acid is much faster than the oxidation of the hydroxyl group (−OH) at position C-6 of D-gluconic acid to L-guluronic acid ($C_6H_{10}O_7$, 193.03 *m/z*), (ROH → RCHO → RCOOH). However, the MS signal at *m/z* 193.03 might belong to the D-glucuronic acid. Indeed, D-glucuronic acid in a cyclic pyranose form (Scheme 1) can also be generated *via* direct oxidation of glucose on a C-6 carbon atom that may also refer to the same MS signal at *m/z* 193.03. 2-Keto- and 5-keto-D-gluconic acids (with the chemical formula of $C_6H_{10}O_7$; 193.03 *m/z*) can be generated *via* oxidation of 2-keto-D-glucose {$[C_6H_{10}O_6{-}H]^-$; 177.04 *m/z*} and/or directly *via* D-gluconic acid. Oxidation of the aldehyde (−CHO) group of 2-keto-D-glucose to produce the 2-keto-D-gluconic acid might be faster than the oxidation of the primary alcohol (−OH) group of gluconic acid to produce L-guluronic acid. Nevertheless, it is expected that the MS signal at *m/z* 193.03 belongs mainly to the L-guluronic acid, which could further transform to D-glucaric acid *m/z* 255.06 {$[C_6H_{10}O_8$ + CHOO]$^-$, observed}. It is essential to mention that the oxidation of an aldehyde (−CHO) group of L-guluronic acid to D-glucaric acid {$[C_6H_{10}O_8{-}H]^-$; 209.03 *m/z*} is in accordance with the general knowledge of aldehyde chemistry. However, the D-glucaric acid production with the C-

https://doi.org/10.1021/acsomega.2c02965
ACS Omega 2022, 7, 31983−31998

Table 1. Observed D-Glucose and D-Glucose-$^{13}C_6$ Oxidation Modifications After Plasma Treatments Monitored by High-Resolution Mass Spectrometry and Tandem Mass Spectrometry

m/z values ^{12}C (^{13}C)	MS/MS values[a] ^{12}C (^{13}C)	molecular ions (generic names)
195.04 (201.06)	129.01, 75.00, 59.01	$[C_6H_{12}O_7-H]^-$ (D-gluconic acid)[g]
195.04[b] (200.06)[c]	(134.03, 77.01, 61.01)[c]	$[C_5H_{10}O_5 + CHOO]^-$
193.03 (199.05)	165.03, 147.02, 113.01, 59.01 (170.05, 152.04, 118.03, 61.01)	$[C_6H_{10}O_7- H]^-$ (D-glucuronic acid)[g]
177.03 (183.05)	159.02, 129.01, 117.01, 99.00, 87.00, 71.00, 59.01	$[C_6H_{10}O_6-H]^-$ (2-keto-D-Glucose)[g], (glucono-1,4-lactone)[g]
177.03[b] (182.04)[d]	(165.04, 134.03, 103.01, 90.01, 74.02, 61.01)	$[C_5H_8O_4 + CHOO]^-$
165.03 (170.05)	149.00, 133.00, 89.01, 75.00, 71.00	$[C_5H_{10}O_6-H]^-$ (D-ribonic acid)
165.03[b] (169.04)	(152.04, 134.03, 77.01, 61.01)	$[C_4H_8O_4 + CHOO]^-$
163.01 (168.03)	101.01, 73.00 (105.03, 75,00)	$[C_5H_{12}O_5-H]^-$ (D-arabinuronic acid)
159.04 (165.04)	129.00, 99.00, 85.00 (134.03, 103.01, 89.03)	$[C_6H_8O_5-H]^-$ (2-oxoadipic acid)
133.01 (138.05)[d]	89.00, 71.00, 59.01	$[C_5H_{10}O_4-H]^-$ (3-deoxy-D-ribose)[g]
129.01 (134.03)	85.00, 57.00 (89.03, 60.04)	$[C_5H_6O_4-H]^-$ (glutaconic acid)[g]
87.01 (90.01)	73.00, 59.01, 41.00 (75.00, 61.01, 43.00)	$[C_3H_4O_3-H]^-$ (glucic acid)
209.03[d] (215.03)[d]	191.01, 129.01, 117.01, 103.00, 87.00, 59.01[e]	$[C_6H_{10}O_8-H]^-$ (D-glucaric acid)
255.06[b] (261.08)	(183.05, 165.04, 134.03, 121.02, 90.01, 77.01)	$[C_6H_{10}O_8 + CHOO]^-$
223.04[f] (229.06)	177.03, 159.02, 129.01, 99.00, 87.00	$[C_7H_{12}O_8-H]^-$ (esterified D-glucaric acid)
223.04[b] (229.06)	(183.05, 165.04, 134.03, 103.01, 90.01)	$[C_6H_{10}O_6 + CHOO]^-$

[a]See Supporting Information Figure S14 for more details. [b]Ionization with formate anion. [c]Observed only after 5−10 min plasma treatment. [d]Observed only after plasma treatment with the $Ar/O_2 + N_2$ curtain gas regime. [e]Very weak MS signals. [f]Esterification product in the presence of methanol in solution. [g]Product identity monitored by comparison with authentic compounds.

6 dicarboxylic acid chain-terminating function was not observed at m/z 209.03. Instead, it was detected at m/z 255.06, most likely due to its tendency to ionize with formate anion as $[C_6H_{10}O_8 + CHOO]^-$ during ionization.

The oxidation chemistry of the secondary alcohol on the C-2 position of glucose could lead to the production of 2-keto-D-glucose ($C_6H_{10}O_6$, 177.03 m/z). The MS signal at m/z 177.03 might also belong to glucono-1,4- and 1,5-lactone (intermolecular dehydration pathway of gluconic acid) (Scheme 1). Notably, the glucono-1,4-lactone ($C_6H_{10}O_6$, 177.04 m/z) is thermodynamically more stable than glucono-1,5-lactone ($C_6H_{10}O_6$, 177.04 m/z), which was reported to more easily rehydrolyze.[33] It is known from the literature that the glucono-1,5-lactone can hydrolyze in an aqueous solution to gluconic acid spontaneously at acidic pH.[33] However, the susceptibility of D-glucose and its oxidation products to CAP-induced ROS led to a complex mixture, the deciphering the full oxidation mechanism is challenging. Nevertheless, our findings show that the three identified oxidation products m/z 195.04, 193.03, and 177.03 are more predominant than other oxidation products after plasma treatment, with the denoted gas variations as shown in Figure 2. Comparison with authentic compounds (tandem mass spectrometry analysis) proved the presence of later-mentioned oxidation products (Supporting Information Figures S15−S20). The abundance of oxidation products will be discussed in detail in the subsequent section. The MS signal at m/z 159.04 might belong to the 2-oxoadipic acid ($C_6H_8O_5$), which is in accordance with the m/z value of the D-glucose-$^{13}C_6$ solution at m/z 165.04. Other glucose oxidation products observed have less than six carbons indicating a subsequent C−C bond cleavage except for a signal at m/z 223.04 (see Table 1). The MS signal at m/z 223.04 might belong to the methanol esterified D-glucaric acid ($C_7H_{12}O_8$) in solution or $[C_6H_{10}O_6 + CHOO]^-$. The MS signals at m/z 165.03 ($C_5H_{10}O_6$), m/z 163.01 ($C_5H_{12}O_5$), m/z 133.0 ($C_5H_{10}O_4$), and m/z 87.01 ($C_3H_4O_3$) are likely attributable to D-ribonic acid, D-arabinuronic acid, 3-deoxy-D-ribose, and glucic acid, respectively (see Scheme 1 for chemical structures). The MS signal at m/z 129.01 (glutaconic acid, $C_5H_6O_4$) was also observed, along with the corresponding MS signal at m/z 134.03 in D-glucose-$^{13}C_6$ oxidation. The signal m/z 87.01 might belong to D-glucic acid as a dialdehyde product of glucose oxidation.

Less-abundant products at m/z 209.02, 191.01, and 175.03 were also detected by applying $Ar/O_2 + N_2$ curtain gas for 10 min, as labeled with the star symbol in Figure 3.

Molecular ions analysis of less-abundant oxidation products is listed in Table 2. The D-glucaric acid, as a further oxidation product of L-guluronic or D-glucuronic acid, is in equilibrium with D-glucaro-lactones (1,4- and 3,6-lactone) at m/z 191.03 {$[C_6H_8O_7-H]^-$}, (see Scheme 1). A similar MS signal at m/z 197.03 was also observed after treating the D-glucose-$^{13}C_6$ solution (see Supporting Information). Nevertheless, the formation of D-glucaro-1,4-3,6-dilactone was not observed in the MS spectra of D-glucose and D-glucose-$^{13}C_6$ solutions after plasma treatment with the $Ar/O_2 + N_2$ curtain gas regime. It is reported that only a minor amount of mono oxo-D-gluconic acids are products of D-glucose oxidation in basic conditions,[60] which is different from the expected pH range after plasma treatment. Nonetheless, we cannot exclude the formation of 2,5-dioxo-D-gluconate (191.03 m/z) from 2-oxo- and 5-oxo-D-gluconic acid. The MS signal at m/z 175.03 might belong to the D-glucurono-1,4- and −3,6-lactone and L-gulurono-6,3-lactone (all with the unique chemical formula as $C_6H_8O_6$) as depicted in Scheme 1, which corresponds to a similar MS signal at m/z 181.04 in D-glucose-$^{13}C_6$ solution {$[C_6H_8O_6-H]^-$; see Supporting Information}. However, the glucurono-lactone {$[C_6H_8O_6-H]^-$; 175.03 m/z} is partially ionized with formate anion and observed at m/z 220.14 {$[C_6H_8O_6 + CHOO]^-$} during ionization. It is necessary to point out that the L-gulurono-6,3-lactone is in equilibrium with L-guluronic acid and D-glucuronic acid, while D-glucurono-1,4- and −3,6-lactone is in equilibrium with D-glucuronic acid. Furthermore, adipic acid {$[C_6H_{10}O_4-H]^-$; 145.00 m/z} as the product of complete dehydration of D-glucaric acid (209.04 m/z) was also observed after 10 min plasma treatment with the denoted gas variations, which is more predominant after plasma treatment with $Ar/O_2 + N_2$ curtain gas. Adipic acid production was even

https://doi.org/10.1021/acsomega.2c02965
ACS Omega 2022, 7, 31983−31998

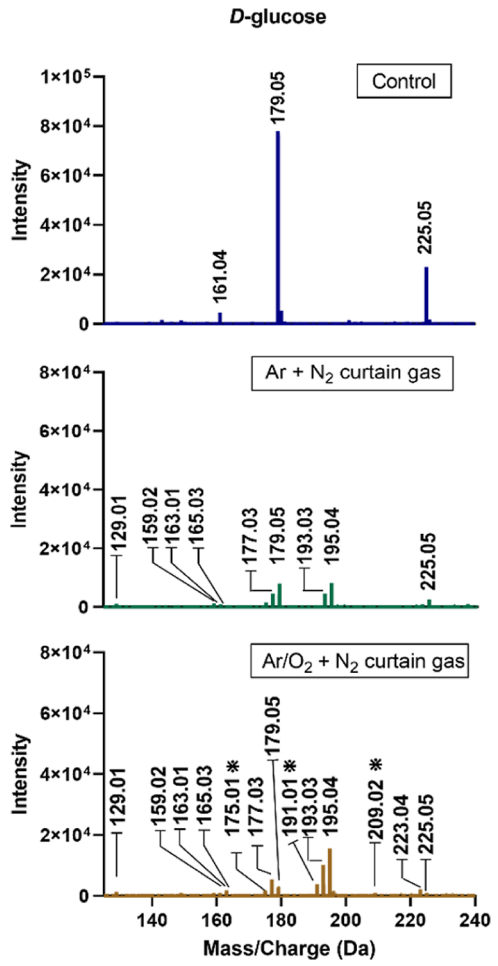

Figure 3. High-resolution mass spectra of D-glucose solution after plasma treatment for 10 min. Plasma gas variations, including Ar discharge and Ar/O_2 admixture coupled with N_2 curtain gas to treat samples as shown with the surrounded box (see method section for details). * Less-abundant MS signals that were only observed after 10 min plasma treatment with Ar discharge only and $Ar/O_2 + N_2$ curtain gas regimes.

Table 2. Molecular Ions Analysis of Less-Abundant Oxidation Products Derived From Plasma Treatment With the $Ar/O_2 + N_2$ Curtain Gas Regime

m/z values ^{12}C (^{13}C)	molecular ions	*m/z* values ^{12}C (^{13}C)	molecular ions
191.03 (231.07)	$[C_6H_8O_7-H]^-$	145.00 (151.00)[a]	$[C_6H_{10}O_4-H]^-$
175.03 (181.04)	$[C_6H_8O_6-H]^-$	220.14 (226.05)[a]	$[C_6H_8O_6+CHOO]^-$

[a]Not observed.

lower than glucaric acid production, which was also detected at *m/z* 255.06 $\{[C_6H_{10}O_8 + CHOO]^-\}$. However, related MS signals in the D-glucose-$^{13}C_6$ spectra were not identified for the two later-mentioned oxidation products. As discussed above and known in the literature, the oxidation of D-glucose to D-glucaric acid requires specific conditions, for example, catalysts, extremes of pH or temperature, and O_2 pressure, which is slow and difficult.[61]

Plausible fragmentation patterns of both D-glucose and D-glucose-$^{13}C_6$ in high-resolution mass spectra are also shown in Table 3. According to Domon and Costello's analyzing

Table 3. Fragmentation Pattern Analysis of D-Glucose Oxidation Products Yielding From the CAP-Induced Reactive Species Impact (Performed *via* Comparing the MS Signal of D-Glucose-$^{13}C_6$ Samples and 1:1 (v/v) Mixture of D-Glucose:D-Glucose-$^{13}C_6$)

m/z values ^{12}C (^{13}C)	molecular ions	*m/z* values ^{12}C (^{13}C)	molecular ions
225.05 (231.07)	$[C_6H_{12}O_6+ CHOO]^-$	113.02 (118.03)	$[C_5H_6O_3-H]^-$
179.05 (185.07)	$[C_6H_{12}O_6-H]^-$	103.03 (107.03)	$[C_4H_8O_3-H]^-$
161.04 (167.06)	$[C_6H_{10}O_5-H]^-$	101.02 (105.03)	$[C_4H_7O_3-H]^-$
149.04 (154.05)	$[C_5H_{10}O_5-H]^-$	99.00 (104.00)[a]	$[C_5H_8O_2-H]^-$
143.03 (149.05)	$[C_6H_8O_4-H]^-$	95.01 (100.02)	$[C_5H_4O_2-H]^-$
141.01 (145.02)	$[C_4H_5O_5-H]^-$	91.05 (94.05)	$[C_3H_8O_3-H]^-$
131.03 (136.04)	$[C_5H_8O_4-H]^-$	89.02 (92.02)	$[C_3H_6O_3-H]^-$
121.02 (125.05)[a]	$[C_4H_{10}O_4-H]^-$	85.02 (90.02)	$[C_5H_{12}O-H]^-$
		85.02 (89.03)	$[C_4H_7O_2-H]^-$
119.03 (123.03)	$[C_4H_8O_4-H]^-$	71.01 (74.01)	$[C_3H_4O_2-H]^-$
117.01 (123.01)	$[C_6H_{14}O_2-H]^-$	73.00 (75.00)	$[C_2H_2O_3-H]^-$
115.03 (120.04)	$[C_5H_8O_3-H]^-$	59.01 (61.01)	$[C_2H_4O_2-H]^-$

[a]Not observed.

method,[62] several fragmentation patterns can be considered due to the formation of X/A ions (C−C bond cleavage) at different ring positions. For instance, the formation of *m/z* 119.02 is related to either the 0,1 or 4,5 glucose ring cleavage, which is in accordance with the previous study.[56] The proposed cross-linked cleavage of D-glucose, D-gluconic acid, and D-glucaric acid are summarized in Scheme S1. On the other hand, utilizing MS/MS analyses, as shown in Figure S21, we identified the fragmentation (daughter) products by changing the collision energy from the parent D-glucose molecule. The fingerprint ionization of D-glucose (*m/z* 179.04) by considering the total carbon atoms proved fragmentations pattern compared with D-glucose-$^{13}C_6$ at *m/z* 185.07. The main fragment ions were detected at *m/z* 89.01 (D-glucose-$^{13}C_6$ isotope: 92.03) and *m/z* 59.01 ($^{13}C_6$ isotope: 61.01) corresponded to $[C_3H_6O_3]^-$ and $[C_2H_3O_2]^-$, respectively.

However, the reaction mechanism was further elucidated using ESI-MS/MS analysis of pure commercially available oxidation modifications to quantify oxidation modifications as postulated in Scheme 1. Hence, the pure form of significant oxidation modification products was measured by high-resolution mass spectrometry and compared with the mass spectra of D-glucose oxidation products in solution after plasma treatment. To gain further mechanistic insight into the oxidation cascade induced by CAP, the ESI-MS/MS spectra were further recorded and compared with plasma-treated samples by adjusting the main MS/MS signals (Supporting Information Figure S22).

Abundance of D-Glucose Oxidation Products. In order to gain insight into the impact of CAP-driven oxidation, modulated by gas mixtures, N_2 shielding, exposure times on the occurrence of dominant oxidation products, and relative

https://doi.org/10.1021/acsomega.2c02965
ACS Omega 2022, 7, 31983−31998

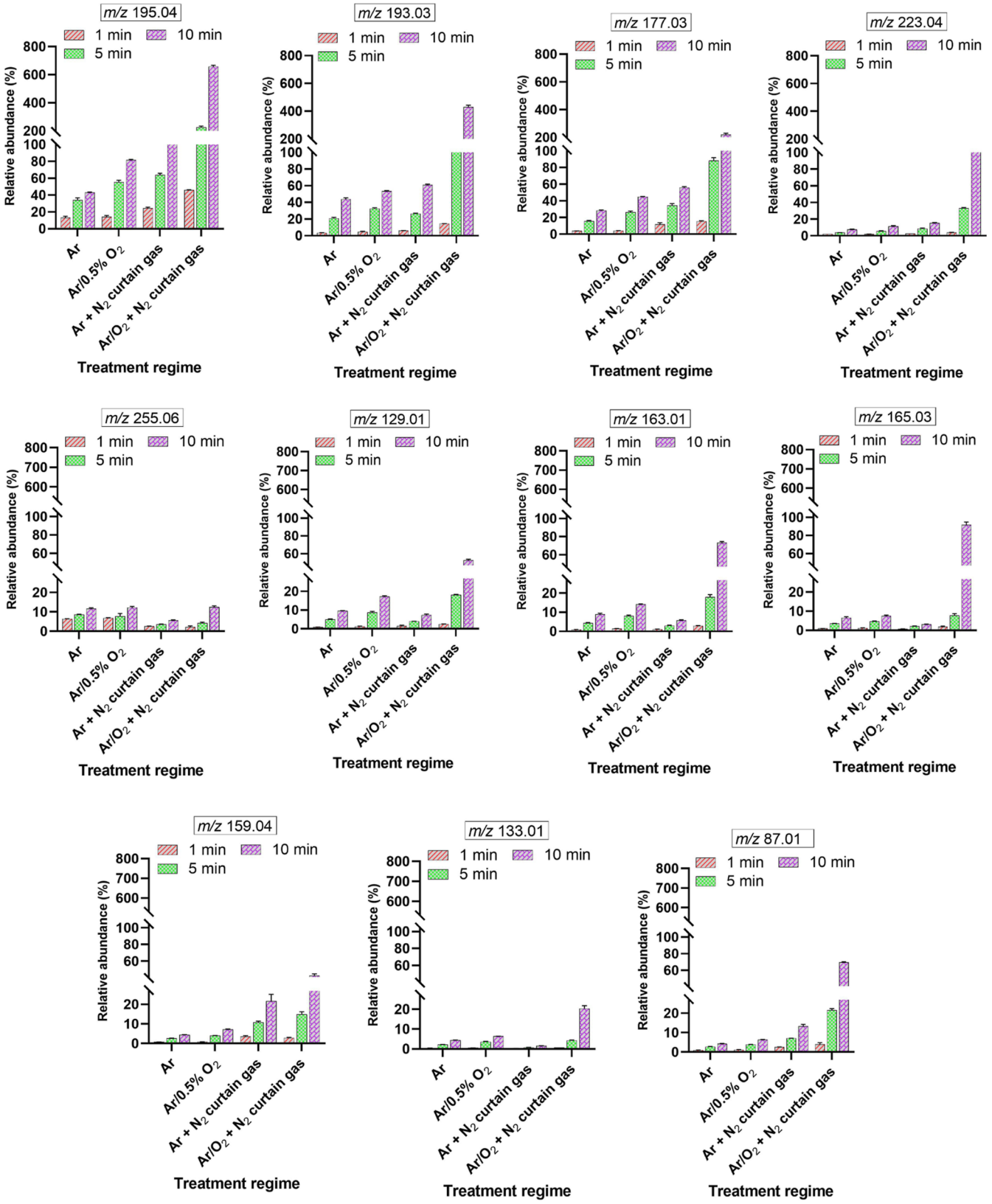

Figure 4. Relative abundances of D-glucose oxidation products (see Scheme 1 for details) after plasma treatment with the denoted gas variations from 1 to 10 min. After plasma treatments, the percentage of oxidation modifications is defined as the peak area of each oxidation modification quantified in each sample relative to the peak area of nonoxidized glucose $[C_6H_{12}O_6-H]^-$ at *m/z* 179.05.

abundances were analyzed. The peak area of the molecule ion at *m/z* 179.05 (185.07 for D-glucose-$^{13}C_6$) was used to calculate the relative abundance of observed oxidation product ions in percent (%, Figure 4 and in the Supporting Information Figure S23).

https://doi.org/10.1021/acsomega.2c02965
ACS Omega 2022, 7, 31983−31998

This approach visualizes differences/similarities in the underlying oxidation mechanisms dependent on the plasma conditions.[63] As expected, the abundance of the oxidation products increased with treatment time, regardless of gas-phase composition. The argon-only condition showed the weakest impact when compared to all other conditions. Using a N_2 curtain around the Ar discharge yielded increased product abundance, corresponding to the preservation of gas-phase species by avoiding their collision with ambient oxygen molecules. Likewise, an admixture of 0.5% O_2 to the feed gas led to an overall increase of oxidation products, indicating a more substantial oxidative impact due to a higher yield of pro-oxidant reactive species than the Ar-only condition. If the N_2 curtain is used additionally, this condition yielded the highest consumption of glucose and subsequent oxidation product abundance (Figure 4). Clearly, the strong formation of atomic oxygen and singlet oxygen in the gas phase, combined with the protective nitrogen curtain, allowed the highest densities of ROS in the interface region and the liquid. The relative abundances of MS signals at *m/z* 195.04, 193.03, and 177.03 were boosted under highly oxidizing treatment conditions (O_2 admixture and shielding). D-gluconic acid at *m/z* 195.04 increased about 8-fold after applying the Ar/O_2 + N_2 curtain gas compared to Ar/O_2 admixture alone (10 min treatment). The abundance of the products at *m/z* 193.03 and 177.03 increased approximately 10-fold and 5-fold, respectively, after applying the N_2 curtain gas to the Ar/O_2. In contrast, their abundances were low for pure Ar discharge conditions. Similar behavior was observed for the products at *m/z* 165.03 and 163.01 that increased about 10-fold and 4-fold, respectively, under Ar/O_2 + N_2 shielding conditions. The oxidation products at *m/z* 159.04 and 133.01 were exclusively observed after 10 min in the Ar/O_2 + N_2 curtain gas. As shown in Figure 4, the abundance of these oxidation products was significant for Ar/O_2 + N_2 curtain gas compared to Ar discharge only, pointing to the higher level of oxygen-derived reactive species in these conditions. In addition, the MS signals at *m/z* 129.01 and 87.01 were increased about 2-fold and 6-fold, respectively, after applying the N_2 curtain gas to the Ar/O_2 admixture regime. Notably, the abundance of D-glucaric acid {$[C_6H_{10}O_8$ + CHOO$]^-$, 255.06 *m/z*} remained independent of the N_2 curtain (Figure 4). This observation might indicate a role for reactive nitrogen species, which are suppressed by the N_2 curtain, or decay reactions that are facilitated by atomic oxygen/singlet oxygen. Interestingly, only trace amounts of glucarolactones (191.01 *m/z*) and gulurunolactones (175.03 *m/z*) were observed after plasma treatment under the pure Ar discharge (Figure 5). At the same time, their abundance was significantly higher after plasma treatment with Ar/O_2 + N_2 curtain gas regime. This phenomenon is most likely due to the higher pH level of solution after plasma treatment that facilitated the dehydration reaction of corresponded oxidized products (see Scheme 1). An admixture of O_2 (plus shielding with N_2) led to a significant increase of signals at *m/z* 209.04 and 193.03, pinpointing strong oxidant ROS responsible for their occurrence and further dehydration reactions. As shown in Figure 5, no significant change was observed in the abundance of glucuronolactone ionized with the formate anion (220.14 *m/z*). In comparison, the abundance of adipic acid (145.01 *m/z*) was significantly increased under the Ar/O_2 + N_2 curtain gas regime. The observed D-glucose oxidation product abundancies indicated a significant role of oxygen-derived reactive oxygen species in solution that will be discussed in the subsequent section. Although we expected that the atomic oxygen [O(3P)] and hydroxyl radical ($^{\bullet}$OH) could be involved in glucose oxidation due to their higher production, in particular, in the oxygen-enriched plasma effluent that is shielded with N_2 flow. However, the D-glucose consumption and D-gluconic acid production were monitored after plasma treatment by plotting calibration curves of authentic compounds at *m/z* 179.05 (D-glucose) and *m/z* 195.04 (D-gluconic acid), respectively. As shown in Figure S24, the glucose concentration was decreased below 100 μM under the Ar/O_2 + N_2 curtain gas regime (treatment time: 10 min), while only 10−20 μM of D-gluconic acid was detected in the same treatment condition.

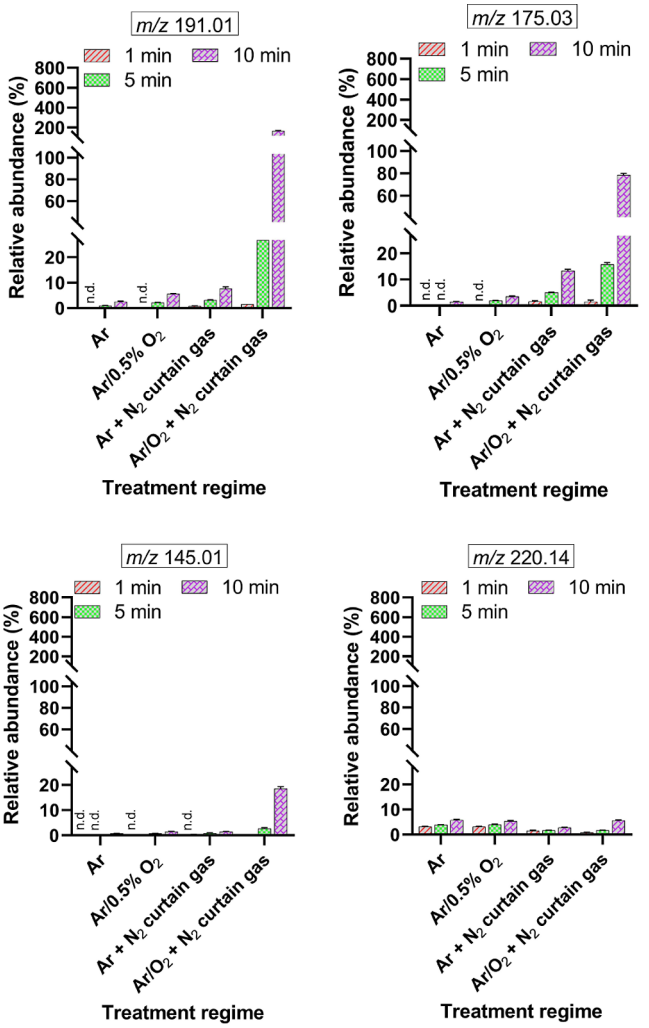

Figure 5. Relative abundances of D-glucose oxidation products after plasma treatment with the denoted gas variations from 1 to 10 min. After plasma treatments, the percentage of oxidation modifications is defined as the peak area of each oxidation modification quantified in each sample relative to the peak area of nonoxidized glucose $[C_6H_{12}O_6-H]^-$ at *m/z* 179.05. Note: the oxidation modifications at *m/z* 191.01, 175.03, and 145.00 were not observed after 1 min plasma treatment with Ar discharge and Ar/O_2 admixture regimes. n.d. = not determined.

CAP-Induced Reactive Species Chemistry. CAP generates a high amount of various short- and long-lived reactive species. *Via* transport processes and reactions at the gas−liquid interface, some of these are available for chemical reactions in the liquid bulk or the boundary layer, depending on their

https://doi.org/10.1021/acsomega.2c02965
ACS Omega 2022, 7, 31983−31998

electronic structure and reactivity. Among these, hydrogen peroxide (H_2O_2), hydroxyl radical ($^{\bullet}OH$)/atomic oxygen [O(3P)], and singlet oxygen ($^1O_2$; $a^1\Delta g$) were detected or quantified in this study. In agreement with previous reports, when water was treated with CAP, a high amount of bicarbonate (HCO_3^-), carbonate radicals ($CO_3^{\bullet-}$), and nitrate (NO_3^-) can be produced, which were detected in the recorded mass spectra at *m/z* 61.98, 60.99, and 59.98, respectively. As shown in Table 4, the peak area of HCO_3^- and $CO_3^{\bullet-}$ have

Table 4. Mass Spectra Analysis of 1:1 Ratio (v/v) of D-Glucose:D-Glucose-$^{13}C_6$ Solution After Plasma Treatment Diluted with 1:4 Ratio (v/v) of 20% MeOH in 5 mM of Ammonium Formate at pH 7.4

		CAP treatment regime[a]		
m/z values	chemical formula	control (%)	Ar (%)	Ar/O_2 (%)
61.98	NO_3^-	6	32	9
60.99	HCO_3^-	6	6	6
59.98	$CO_3^{\bullet-}$	100	100	100
44.99	HCO_2^-	75	60	100

[a]The results for 10 min plasma treatment.

remained constant, while other signal percentages were changed by changing the plasma treatment regime. Tresp *et al.*[64] found that both bicarbonate and carbonate in solution could react with $^{\bullet}OH$ to form $CO_3^{\bullet-}$. In addition, nitrite may form due to the interaction of the plasma effluent with ambient air. Therefore, the highest amount of NO_3^- was observed when the treatment regime with only Ar feed gas was applied, which is related to the reaction of nitrite (NO_2^-) in the presence of hydrogen peroxide (H_2O_2). The deposition of nitrite/nitrate was also measured *via* ion chromatography in water and glucose-containing solution. The results showed that by applying the Ar discharge and $Ar/O_2 + N_2$ curtain gas, the maximum amount of NO_2^-/NO_3^- was detected (see Supporting Information Figure S25). CAP treatment of D-glucose solution resulted in relatively higher nitrite levels in all denoted gas variations. However, nitrate production was independent of glucose present in the treated solution.

Notably, formic acid production could be linked to the reaction of CO_2 from the air with oxygen-derived short-lived reactive species (Table 4). It could also refer to its production from D-glucose oxidation (see Supporting Information Figure S26).

In the first step, plasma's effect on producing H_2O_2 as the main long-life reactive species present in the liquid bulk was investigated in water and 2 mM of D-glucose solution. As shown in Figure 6a, the concentration of H_2O_2 in D-glucose solutions was significantly higher after 5 and 10 min plasma, irrespective of the feed gas composition. Relatively high concentrations of H_2O_2 were deposited by treating the sample with Ar feed gas in a time-dependent manner. In the presence of D-glucose, up to about 750 μM after plasma treatment for 10 min were detected, while in pure water, only 490 μM were observed. In contrast, an H_2O_2 concentration of about 550 μM was determined in D-glucose solutions treated with $Ar/O_2 + N_2$ curtain gas for 10 min, while in pure water, only 100 μM were deposited at the same time (Figure 6a). This indicates the production of H_2O_2 as the by-product of CAP-induced D-glucose oxidation or a reduced decay *via* O/OH radicals forming superoxide anion radicals that are disproportionate to H_2O_2 and water. To confirm our suggestion, more experiments were conducted by measuring the amounts of produced H_2O_2 during the treatments of solutions containing various D-glucose concentrations. As shown in Figure 6b, increasing the glucose concentration led to the significant enhancement of produced H_2O_2 during 5 min plasma treatment under the $Ar/O_2 + N_2$ curtain gas regime compared to only Ar discharge. The concentration of produced H_2O_2 almost remained constant by treatment of D-glucose solutions more concentrated than 8 mM under $Ar/O_2 + N_2$ curtain gas due to the available molecular level of glucose and CAP-induced oxidant per plasma exposure period, while the produced H_2O_2 from the Ar treatment at the same solution remained constant and independent of the D-glucose concentrations for solutions containing more than 1 mM D-glucose. This phenomenon not only proved that the glucose oxidizes effectively by plasma treatment with $Ar/O_2 + N_2$ curtain gas regime but is also related to glucose utilization for the *in situ* production of H_2O_2 in the oxidation cascade. For $Ar/O_2 + N_2$ curtain gas treatment, the highest concentration of H_2O_2 coaligns with the highest glucose consumption. It has been shown that hydroperoxyl radicals ($^{\bullet}OOH$) are formed during glucose oxidation, which in low pH convert to H_2O_2 ($^{\bullet}OOH + {}^{\bullet}O_2^- + H^+ \rightarrow H_2O_2 + O_2$).[65] Therefore, it might be hypothesized that both *in vitro* and *in vivo*, a local increase in $^{\bullet}OOH$ and H_2O_2 formation may result from carbohydrate, especially the D-glucose, oxidation due to plasma treatment. Subsequent effects on biomolecules and signal cascades, especially in the presence of catalysts or free thiols, should be considered.

On the other hand, it is known that the relatively mild oxidizing reagent H_2O_2 oxidizes D-glucose only in the presence of an appropriate (metal) catalyst.[66,67] In the absence of such, H_2O_2 (100, 500, and 1000 μM) did not oxidize D-glucose in solution (measured pH value = 6.4; see Supporting Information Figures S27 and S28). In the following, irradiation of H_2O_2 in the VNIR range as emitted from Ar discharge equipped with a borofloat-33 window to photolytically cleave H_2O_2 to $^{\bullet}OH$ either did not take place/or was too small extend to oxidize the glucose (Figure S29).

As shown in Supporting Information Figure S30, no H_2O_2 formation was determined using borofloat-33 (UV-A and visible lights; transparent >100 nm). In contrast, H_2O_2 concentration was determined at about 10−20 μM in the presence of VUV radiation using the MgF_2 window (transparent >100 nm). The results suggest that the VUV radiation has a small contribution to H_2O_2 production compared to deposited H_2O_2 induced by CAP-generated reactive species in solution. The VUV photolysis is partially involved in the production of a small amount of $^{\bullet}OH$ and consequently H_2O_2 *via* reactions R1−R3.[68,69] Parallel to the abovementioned experiments, the impact of CAP-activated water solutions was studied by its addition to the D-glucose solution. Only trace amounts of D-gluconic acid and D-glucaric acid (*m/z* 195.05 and 255.23) were observed (Supporting Information Figure S31), whereas H_2O_2 deposition was only significant after plasma treatment with only Ar discharge. This result shows that short-lived reactive species such as $^1O_2$, $^{\bullet}OH$, and $O(^3P)$ are engaged in the glucose oxidation cascade and that H_2O_2 is a by-product of this process.

In nonthermal plasma liquid chemistry, the molecular O_2 in the gas phase can mainly generate a large amount of metastable $O(^3P)$ and superoxide ($^{\bullet}O_2^-$) that can travel to the surface (R4−R6). Ozone photolysis can slightly contribute due to its related slow dissolution in water when using O_2 as admixture

https://doi.org/10.1021/acsomega.2c02965
ACS Omega 2022, 7, 31983−31998

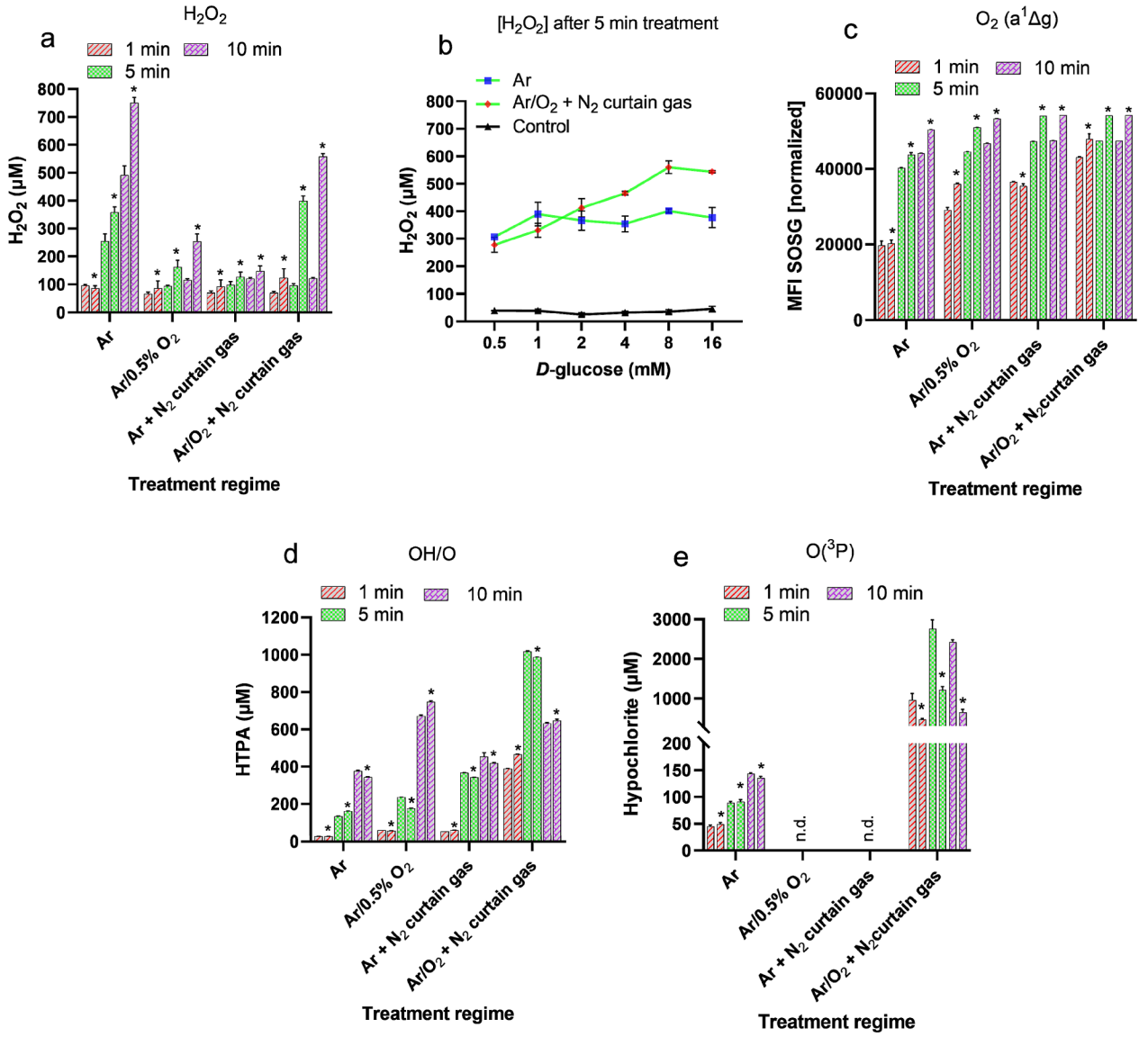

Figure 6. Reactive species profiles after plasma treatment. (a) H_2O_2 concentration determination directly after plasma treatment in water and D-glucose solution, (b) H_2O_2 concentration determination after 5 min plasma treatment by varying the D-glucose concentration in solution, (c) $O_2(a\,^1\Delta g)$ quantification using the SOSG Assay Kit, (d) $^{\bullet}OH/O(^3P)$ concentration in liquid media *via* conversion of TPA to HTPA in phosphate buffer (TPA assay), (e) $O(^3P)$ profile by following the concentration of hypochlorite (ClO^-) in PBS *via* electrochemical sensing. *2 mM D-glucose solution samples. n.d. = not determined.

gas (R7 and R8). However, both sources of $O(^3P)$ can involve in the formation of $^{\bullet}OH$ (R9).[44] For the kINPen, high concentrations of the aforementioned short-lived oxygen-derived reactive species are produced mainly in the Ar/O_2 admixture plus N_2 curtain gas.[44] The radical reaction generated during the plasma treatment is shown below

$$H_2O + h\nu \rightarrow H^+ + OH^- \quad (R1)$$

$$OH^- \rightarrow {}^{\bullet}OH + e^- \quad (R2)$$

$$OH + {}^{\bullet}OH \rightarrow H_2O_2 \quad (R3)$$

$$O_2 + e^- \rightarrow {}^{\bullet}O_2^- \quad (R4)$$

$$O_2 + e^- \rightarrow O + O + e^- \quad (R5)$$

$$O + e^- \rightarrow O(^3P) + e^- \quad (R6)$$

$$O + O_2 \rightarrow O_3 \quad (R7)$$

$$O_3 + h\nu \rightarrow O_2 + O(^3P) \quad (R8)$$

$$O(^3P) + H_2O \rightarrow 2{}^{\bullet}OH \quad (R9)$$

$$^{\bullet}O_2^- \rightarrow {}^1O_2 + e^- \quad (R10)$$

$$^{\bullet}O_2^- + H_2O_2 \rightarrow {}^1O_2 + {}^{\bullet}OH + OH^- \quad (R11)$$

$$^{\bullet}O_2^- + {}^{\bullet}OH \rightarrow {}^1O_2 + OH^- \quad (R12)$$

It is known from CAP chemistry that N_2 curtain gas prevents the quenching of $^1O_2$, and $O(^3P)$ by collision with ambient O_2 molecules, and in this condition, gas–liquid interface densities are the highest. Conversely, an O_2 curtain decreases their densities.[44] $^{\bullet}O_2^-$ that is generated in the discharge and may additionally be formed during glucose oxidation contributes to

https://doi.org/10.1021/acsomega.2c02965
ACS Omega 2022, 7, 31983−31998

several reactions (R10−R12) to produce $^1O_2$.[70] By using SOSG, relative quantification of $^1O_2$ was achieved and revealed a slightly time- and working gas composition-dependent formation (Figure 6c). However, the dynamic is less impressive than for H_2O_2. The most prominent $^1O_2$ production was detected after 10 min Ar/O_2 plasma treatment using N_2 curtain gas, parallel with a strong $^•OH/O(^3P)$ deposition (see Figure 6d,e). In the presence of D-glucose, $^1O_2$ deposition was slightly increased, excluding a direct role of $^1O_2$ for D-glucose oxidation (Figure 6c). However, it should be kept in mind that SOSG is under debate, and the chosen approach allowed a relative quantification only. The data allow the assumption that a combination of OH/O radicals has a prominent role in D-glucose oxidation.

Gas-phase $O(^3P)$ formation, transport to the gas−liquid interface and the boundary layer, and its conversion to $^•OH$ radicals (R9) were proposed in the literature.[71] Sugars are also known as $^•OH$ scavengers.[72] To explore the role of OH/O radicals in the present experimental setting, the terephthalic acid (TPA) assay was applied to quantify OH/O radicals concentration as previously described.[49] It should be emphasized that the assay is claimed to be specific for OH radicals; however, due to the quick interchangeability of $O(^3P)$ and $^•OH$ in aqueous systems, the selectivity is hampered.[42] Monitoring the concentration of OH/O radicals in pure water was impeded by the poor solubility of TPA, and a phosphate buffer was used instead. As shown in Figure 6d, the $^•OH/O(^3P)$ deposition increased significantly with treatment time and is modulated by the working gas composition. As expected, the highest amount of OH/O radicals was deposited when O_2 was admixed to the feeding gas. When the N_2 curtain is applied, this is even more pronounced. However, irregularities after 10 min of treatment were observed. It must be assumed that the apparently lower deposition of OH/O is due to the attack of the initial product hydroxyterephthalic acid (HTPA) and the subsequent formation of a non-fluorescent product, ultimately resulting in limited linearity of the assay. An alternative explanation would be the loss of $^•OH$ due to recombination, but this is unlikely regarding the negligible H_2O_2 production under these conditions (see Figure 6a). A straightforward treatment time dependence OH/O deposition was observed for a pure Ar discharge. In this case, the assay detects predominantly $^•OH$ radicals generated from the photolysis of water by the argon excimer VUV traveling the noble gas channel to the gas−liquid interface.[19] Of note, the concentration of OH/O radicals in D-glucose solutions remained almost unchanged, seemingly contradicting reports on OH radical-driven oxidation of glucose (Amaniampong *et al.*,[38] Rinsant *et al.*[73]). It should be considered that, in both cases, bulk liquid reactions were described, while in the current CAP-driven oxidation, a decisive role of the interface region must be admitted. This includes transport processes, strict nonequilibrium conditions, and the consumption of the reactive species at the surface. In addition, the reaction between OH/O radicals and TPA is quicker than with glucose due to higher electron densities at the aromatic ring. A contributing role of the higher pH in phosphate buffer on the reaction rate and mechanism shall not be excluded.

In parallel to the abovementioned experiments, to prove the contribution of the short-lived ROS $^1O_2$ and especially $O(^3P)$ on glucose oxidation, the scavenger L-histidine was added to the solution. In this case, the peak area of D-glucose at *m/z* 179.05 remains approximately constant (Supporting Information Figure S33). Instead, the L-histidine signal at *m/z* 154.04 declined. This was especially obvious when the $Ar/O_2 + N_2$ curtain gas regime was applied, indicating a high level of $O(^3P)$ (and $^1O_2$) that reacted with the histidine now. Therefore, we assume that OH/O radical species are the main reactive species involved in D-glucose oxidation. This is reflected in the oxidation products as depicted in Scheme S2. The MS signal at *m/z* 170.05 is most likely generated by reaction with $O(^3P)$ or $^•OH$, generated according to R6. The product of histidine oxidation at *m/z* 187.06 related to the $^1O_2$ scavenging (see Scheme S2) observed when the pure Ar discharge was shielded with N_2 flow. However, as a less relevant generated species by plasma, $^1O_2$ could not directly influence glucose oxidation; nevertheless, $^1O_2$ might undergo the small conversion of H_2O_2 to $^•OH$ and, consequently, D-glucose oxidation in solution.

In an orthogonal approach, the deposition of $O(^3P)$ was determined using its reactivity with chloride ions, yielding hypochlorite (ClO^-) using an electrochemical sensor.[50,74] The experiments were performed in PBS with/without glucose (2 mM). The amount of produced hypochlorite is related to the gas−liquid interface concentration of $O(^3P)$ (Figure 6e). The data confirm the results of the TPA assay, showing a massive increase in hypochlorite production under the $Ar/O_2 + N_2$ curtain gas regime. Interestingly, the ClO^- formation in the presence of glucose shows significant differences between the Ar discharge only and Ar/O_2 admixture with N_2 shielding flow. This difference allows us to conclude that $O(^3P)$, not $^•OH$, plays the main role in glucose oxidation, at least in the $Ar/O_2 + N_2$ curtain gas case: in Ar discharge only, VUV leads to the photolysis of water and subsequently to the formation of OH radicals that react with chloride ions, but not with the glucose, leaving the ClO^- levels unchanged. In contrast, the $O(^3P)$ formed in the Ar/O_2 admixture shielded with the N_2 flow case reacts with chloride ions and glucose, yielding lower ClO^- levels in its presence. It may be assumed that the free traveling path of $O(^3P)$ is larger than for $^•OH$, allowing a reaction with the glucose also in the boundary layer below the gas−liquid interface. Experiments using caged $O(^3P)$ generators support this notion.[75] Again, the strict nonequilibrium conditions of the plasma−liquid interaction must be taken into consideration. In bulk reactions (e.g., H_2O_2 and a catalyst), the situation is different. However, no glucose oxidation products were observed in a control experiment by adding 10 mM of hypochlorite solution to the D-glucose, suggesting that glucose only reacted with $O(^3P)$ and not the hypochlorite. An alternative and/or contributing role can be attributed to the pH during the CAP-driven oxidation. The ClO^- concentrations in PBS (pH ∼ 7.4) and KCl (0.14 M M; pH ∼ 3−4) showed a similar behavior (see Supporting Information Figure S34). This suggests that $O(^3P)$ induced oxidation of D-glucose is not pH-dependent, while the $^•OH$-induced oxidation of D-glucose is pH-dependent.

Although it is hard to interpret the responsible reactive species pattern on D-glucose oxidation by plasma discharges, it can be assumed that depending on the gas phase composition and the treatment regime, a combination of OH/O radicals is responsible. $O(^3P)$ is the primary oxidant of glucose in the case of Ar/O_2 admixture with or without N_2 curtain gas. A more robust oxidative impact yields highly oxidized products with higher yields than the pure Ar discharge in these conditions. This is in accordance with the literature using atmospheric pressure plasma jet with helium as feed gas admixed with oxygen.[76] Benedikt *et al.*[71] also reported that the $O(^3P)$ could

https://doi.org/10.1021/acsomega.2c02965
ACS Omega 2022, 7, 31983−31998

directly oxidize organic molecules. On the contrary, $^{\bullet}$OH radicals are the major responsible oxidants in Ar only discharges of the kINPen, to some extent irrespective of the feed gas. Further investigations are required to fully rationalize the oxidation mechanism using cold plasma.

CONCLUSIONS

In summary, CAP was employed to generate oxygen-derived reactive species oxidizing the model carbohydrate D-glucose, yielding mainly D-gluconic acid at *m/z* 195.04, isobaric products at *m/z* 193.03 with D-glucuronic acid, L-guluronic acid, and 2- or 5-oxo-D-gluconic acid, along with gluconolactones at *m/z* 177.03 and a number of minor products, for example, at *m/z* 255.06 {$[C_6H_{10}O_8 + CHOO]^-$} and *m/z* 209.03 (D-glucaric acid). Up to 90% of the glucose was converted within 10 min when $^1O_2$, $O(^3P)$/ $^{\bullet}$OH were the dominant reactive species (Ar/O_2 conditions with gas shielding). When blocked by the scavenger L-histidine, the glucose conversion rate is significantly decreased. The long-lived species, hydrogen peroxide, is irrelevant for oxidation. These results indicate that carbohydrates are relevant targets for cold plasmas, and given their presence in both *in vitro* and *in vivo* applications of CAP, must be taken into consideration. The formation of secondary hydrogen peroxide and hydroperoxyl radicals during glucose oxidation may lead to local activation of redox signal cascades.

Although further investigations are still required to fully reveal the role of individual reactive species on the glucose oxidation process, our results suggest that a combination of $^{\bullet}$OH/$O(^3P)$ radicals are responsible for the glucose breakdown. Apart from the biomedical implications sparked by the findings, our work suggests future exploitation of cold plasma as nascent environmentally friendly technology for carbohydrate oxidation chemistry to produce valuable aldonic acids and aldaric acids. This subject area is under investigation by our group.

ASSOCIATED CONTENT

Supporting Information

The Supporting Information is available free of charge at https://pubs.acs.org/doi/10.1021/acsomega.2c02965.

Mass spectra of D-glucose after plasma treatment; MS/MS spectra of oxidation products after CAP treatment; mass spectra of standard authentic compounds; MS/MS spectra of D-glucose at *m/z* 179.04 and D-glucose-$^{13}C_6$ at *m/z* 185.07; MS/MS spectra of standard authentic compounds; proposed cross-ring cleavages of D-glucose; relative abundance of D-glucose-$^{13}C_6$ oxidation products; D-glucose oxidation concentration and D-gluconic acid production determinations after plasma treatment; deposition of nitrite/nitrate profile; relative abundance of formic acid production after plasma treatment; mass spectra of D-glucose by direct addition of H_2O_2; pH of solution by direct addition of H_2O_2; mass spectra of D-glucose after direct addition of H_2O_2 (400 μM in solution) that were exposed to Ar discharge regime blocked with borofloat-33 window; H_2O_2 production determination due to VUV/UV transmission to the solution by blocking the gas−liquid interface; deposited H_2O_2 concentration determination after plasma treatment in water; mass spectra of D-glucose after 5 min plasma treatment under denoted gas variations and shielding; schematic illustration of scavenging pathway of L-histidine in D-glucose solutions; and effect of radical scavenger's L-histidine on D-glucose oxidation efficiency in water (PDF)

AUTHOR INFORMATION

Corresponding Authors

Mohsen Ahmadi − *Leibniz Institute for Plasma Science and Technology (INP Greifswald), Center for Innovation Competence (ZIK) plasmatis, Greifswald 17489, Germany;* orcid.org/0000-0002-7018-0460; Email: mohsen.ahmadi@inp-greifswald.de

Kristian Wende − *Leibniz Institute for Plasma Science and Technology (INP Greifswald), Center for Innovation Competence (ZIK) plasmatis, Greifswald 17489, Germany;* orcid.org/0000-0001-5217-0683; Email: kristian.wende@inp-greifswald.de

Authors

Zahra Nasri − *Leibniz Institute for Plasma Science and Technology (INP Greifswald), Center for Innovation Competence (ZIK) plasmatis, Greifswald 17489, Germany*

Thomas von Woedtke − *Leibniz Institute for Plasma Science and Technology (INP Greifswald), Center for Innovation Competence (ZIK) plasmatis, Greifswald 17489, Germany; Leibniz Institute for Plasma Science and Technology (INP Greifswald), Greifswald 17489, Germany; University Medicine Greifswald, Institute for Hygiene and Environmental Medicine, Greifswald 17489, Germany;* orcid.org/0000-0002-1097-4832

Complete contact information is available at: https://pubs.acs.org/10.1021/acsomega.2c02965

Notes

The authors declare no competing financial interest.

ACKNOWLEDGMENTS

This work is funded by the German Federal Ministry of Education and Research (GN: 03Z22DN12 to K.W.).

ABBREVIATIONS

CAP	cold atmospheric plasma
Ar	argon
slm	standard liters per minute
ROS	reactive oxygen species
RONS	reactive oxygen and nitrogen species
TPA	terephatalic acid
HTPA	2-hydroxyterephtalic acid
VUV	vacuum ultraviolet
μM	micromolar
mM	millimolar
MS/MS	tandem mass spectrometry
m/z	mass-to-charge ratio
O_2	oxygen
$^{\bullet}O_2^-$	Superoxide
$O(^3P)$	atomic oxygen
$^{\bullet}$OH	hydroxyl radical
$^1O_2$	singlet oxygen
H_2O_2	hydrogen peroxide
$^{\bullet}$OOH	hydroperoxide radical
O_3	ozone
ClO^-	hypochlorite

https://doi.org/10.1021/acsomega.2c02965
ACS Omega 2022, 7, 31983−31998

NO_2^- nitrite
NO_3^- nitrate

REFERENCES

(1) Arndt, S.; Unger, P.; Wacker, E.; Shimizu, T.; Heinlin, J.; Li, Y. F.; Thomas, H. M.; Morfill, G. E.; Zimmermann, J. L.; Bosserhoff, A. K.; et al. Cold atmospheric plasma (CAP) changes gene expression of key molecules of the wound healing machinery and improves wound healing in vitro and in vivo. *PLoS One* **2013**, *8*, No. e79325.

(2) Bernhardt, T.; Semmler, M. L.; Schäfer, M.; Bekeschus, S.; Emmert, S.; Boeckmann, L. Plasma Medicine: Applications of Cold Atmospheric Pressure Plasma in Dermatology. *Oxid. Med. Cell. Longev.* **2019**, *2019*, 3873928.

(3) Schmidt, A.; Bekeschus, S.; Wende, K.; Vollmar, B.; von Woedtke, T. A cold plasma jet accelerates wound healing in a murine model of full-thickness skin wounds. *Exp. Dermatol.* **2017**, *26*, 156−162.

(4) Duske, K.; Koban, I.; Kindel, E.; Schröder, K.; Nebe, B.; Holtfreter, B.; Jablonowski, L.; Weltmann, K. D.; Kocher, T. Atmospheric plasma enhances wettability and cell spreading on dental implant metals. *J. Clin. Periodontol.* **2012**, *39*, 400−407.

(5) Miebach, L.; Freund, E.; Clemen, R.; Weltmann, K.-D.; Metelmann, H.-R.; von Woedtke, T.; Gerling, T.; Wende, K.; Bekeschus, S. Conductivity augments ROS and RNS delivery and tumor toxicity of an argon plasma jet. *Free Radical Biol. Med.* **2022**, *180*, 210−219.

(6) Tanaka, H.; Bekeschus, S.; Yan, D. Y.; Hori, M.; Keidar, M.; Laroussi, M. Plasma-Treated Solutions (PTS) in Cancer Therapy. *Cancers* **2021**, *13*, 1737.

(7) Bradu, C.; Kutasi, K.; Magureanu, M.; Puač, N.; Živković, S. Reactive nitrogen species in plasma-activated water: generation, chemistry and application in agriculture. *J. Phys. D: Appl. Phys.* **2020**, *53*, 223001.

(8) Pankaj, S. K.; Wan, Z.; Keener, K. M. Effects of Cold Plasma on Food Quality: A Review. *Foods* **2018**, *7*, 4.

(9) Wang, Z.; Zhang, Y.; Neyts, E. C.; Cao, X.; Zhang, X.; Jang, B. W. L.; Liu, C.-j. Catalyst Preparation with Plasmas: How Does It Work? *ACS Catal.* **2018**, *8*, 2093−2110.

(10) Brandenburg, R. Dielectric barrier discharges: progress on plasma sources and on the understanding of regimes and single filaments. *Plasma Sources Sci. Technol.* **2017**, *26*, 053001.

(11) Laroussi, M.; Lu, X.; Keidar, M. Perspective: The physics, diagnostics, and applications of atmospheric pressure low temperature plasma sources used in plasma medicine. *J. Appl. Phys.* **2017**, *122*, 020901.

(12) Reuter, S.; von Woedtke, T.; Weltmann, K. D. The kINPen-a review on physics and chemistry of the atmospheric pressure plasma jet and its applications. *J. Phys. D: Appl. Phys.* **2018**, *51*, 233001−233051.

(13) Privat-Maldonado, A.; Schmidt, A.; Lin, A.; Weltmann, K. D.; Wende, K.; Bogaerts, A.; Bekeschus, S. ROS from Physical Plasmas: Redox Chemistry for Biomedical Therapy. *Oxid. Med. Cell. Longev.* **2019**, *2019*, 9062098.

(14) Von Woedtke, T.; Schmidt, A.; Bekeschus, S.; Wende, K.; Weltmann, K. D. Plasma Medicine: A Field of Applied Redox Biology. *In Vivo* **2019**, *33*, 1011−1026.

(15) Riès, D.; Dilecce, G.; Robert, E.; Ambrico, P. F.; Dozias, S.; Pouvesle, J. M. LIF and fast imaging plasma jet characterization relevant for NTP biomedical applications. *J. Phys. D: Appl. Phys.* **2014**, *47*, 275401.

(16) Bruno, G.; Wenske, S.; Lackmann, J. W.; Lalk, M.; von Woedtke, T.; Wende, K. On the Liquid Chemistry of the Reactive Nitrogen Species Peroxynitrite and Nitrogen Dioxide Generated by Physical Plasmas. *Biomolecules* **2020**, *10*, 1687.

(17) Khlyustova, A.; Labay, C.; Machala, Z.; Ginebra, M.-P.; Canal, C. Important parameters in plasma jets for the production of RONS in liquids for plasma medicine: A brief review. *Front. Chem. Sci. Eng.* **2019**, *13*, 238−252.

(18) Takamatsu, T.; Uehara, K.; Sasaki, Y.; Miyahara, H.; Matsumura, Y.; Iwasawa, A.; Ito, N.; Azuma, T.; Kohno, M.; Okino, A. Investigation of reactive species using various gas plasmas. *RSC Adv.* **2014**, *4*, 39901−39905.

(19) Bruno, G.; Wenske, S.; Mahdikia, H.; Gerling, T.; von Woedtke, T.; Wende, K. Radiation Driven Chemistry in Biomolecules—is (V)UV Involved in the Bioactivity of Argon Jet Plasmas? *Front. Phys.* **2021**, *9*, 759005.

(20) Dubuc, A.; Monsarrat, P.; Virard, F.; Merbahi, N.; Sarrette, J.-P.; Laurencin-Dalicieux, S.; Cousty, S. Use of cold-atmospheric plasma in oncology: a concise systematic review. *Ther. Adv. Med. Oncol.* **2018**, *10*, 1−12.

(21) Klinkhammer, C.; Verlackt, C.; śmiłowicz, D.; Kogelheide, F.; Bogaerts, A.; Metzler-Nolte, N.; Stapelmann, K.; Havenith, M.; Lackmann, J. W. Elucidation of Plasma-induced Chemical Modifications on Glutathione and Glutathione Disulphide. *Sci. Rep.* **2017**, *7*, 13828.

(22) Lackmann, J. W.; Baldus, S.; Steinborn, E.; Edengeiser, E.; Kogelheide, F.; Langklotz, S.; Schneider, S.; Leichert, L. I. O.; Benedikt, J.; Awakowicz, P.; et al. A dielectric barrier discharge terminally inactivates RNase A by oxidizing sulfur-containing amino acids and breaking structural disulfide bonds. *J. Phys. D: Appl. Phys.* **2015**, *48*, 494003.

(23) Attri, P.; Park, J. H.; De Backer, J.; Kim, M.; Yun, J. H.; Heo, Y.; Dewilde, S.; Shiratani, M.; Choi, E. H.; Lee, W.; et al. Structural modification of NADPH oxidase activator (Noxa 1) by oxidative stress: An experimental and computational study. *Int. J. Biol. Macromol.* **2020**, *163*, 2405.

(24) Nasri, Z.; Memari, S.; Wenske, S.; Clemen, R.; Martens, U.; Delcea, M.; Bekeschus, S.; Weltmann, K.-D.; Woedtke, T.; Wende, K. Singlet-Oxygen-Induced Phospholipase A2 Inhibition: A Major Role for Interfacial Tryptophan Dioxidation. *Chem.—Eur. J.* **2021**, *27*, 14702−14710.

(25) Li, Y.; Friedman, G.; Fridman, A.; Ji, H.-F. Decomposition of sugars under non-thermal dielectric barrier discharge plasma. *Clin. Plasma Med.* **2014**, *2*, 56−63.

(26) Sole-Marti, X.; Vilella, T.; Labay, C.; Tampieri, F.; Ginebra, M. P.; Canal, C. Thermosensitive hydrogels to deliver reactive species generated by cold atmospheric plasma: a case study with methylcellulose. *Biomater. Sci.* **2022**, *10*, 3845.

(27) Isikgor, F. H.; Becer, C. R. Lignocellulosic biomass: a sustainable platform for the production of bio-based chemicals and polymers. *Poly. Chem.* **2015**, *6*, 4497−4559.

(28) Mehltretter, C. L.; Rist, C. E. Oxidation, Saccharic and Oxalic Acids by the Nitric Acid Oxidation of Dextrose. *J. Agr. Food Chem.* **1953**, *1*, 779−783.

(29) Kornecki, J. F.; Carballares, D.; Tardioli, P. W.; Rodrigues, R. C.; Berenguer-Murcia, Á.; Alcántara, A. R.; Fernandez-Lafuente, R. Enzyme production of d-gluconic acid and glucose oxidase: successful tales of cascade reactions. *Catal. Sci. Technol.* **2020**, *10*, 5740−5771.

(30) Liu, W.-J.; Xu, Z.; Zhao, D.; Pan, X.-Q.; Li, H.-C.; Hu, X.; Fan, Z.-Y.; Wang, W.-K.; Zhao, G.-H.; Jin, S.; et al. Efficient electrochemical production of glucaric acid and H2 via glucose electrolysis. *Nat. Commun.* **2020**, *11*, 265.

(31) Chen, J.; Ma, Q.; Li, M.; Chao, D.; Huang, L.; Wu, W.; Fang, Y.; Dong, S. Glucose-oxidase like catalytic mechanism of noble metal nanozymes. *Nat. Commun.* **2021**, *12*, 3375.

(32) Aggarwal, N.; Aadil Yatoo, M.; Saravanamurugan, S. Glucose oxidation to carboxylic products with chemocatalysts. In *Biomass, Biofuels, Biochemicals*, Saravanamurugan, S., Pandey, A., Li, H., Riisager, A., Eds.; Elsevier, 2020; pp 33−60 Chapter 2

(33) Armstrong, R. D.; Hirayama, J.; Knight, D. W.; Hutchings, G. J. Quantitative Determination of Pt- Catalyzed d-Glucose Oxidation Products Using 2D NMR. *ACS Catal.* **2019**, *9*, 325−335.

(34) Moggia, G.; Kenis, T.; Daems, N.; Breugelmans, T. Electrochemical Oxidation of d-Glucose in Alkaline Medium: Impact of Oxidation Potential and Chemical Side Reactions on the Selectivity to d-Gluconic and d-Glucaric Acid. *ChemElectroChem* **2020**, *7*, 86−95.

https://doi.org/10.1021/acsomega.2c02965
ACS Omega 2022, 7, 31983−31998

(35) Xu, S.; Minteer, S. D. Enzymatic Biofuel Cell for Oxidation of Glucose to CO2. *ACS Catal.* **2012**, *2*, 91−94.
(36) Honnorat, B.; Brüser, V.; Kolb, J. F. Microwave plasma discharges for biomass pretreatment: Degradation of a sodium carboxymethyl cellulose model. *Aip. Adv.* **2020**, *10*, 095025.
(37) Vizireanu, S.; Panaitescu, D. M.; Nicolae, C. A.; Frone, A. N.; Chiulan, I.; Ionita, M. D.; Satulu, V.; Carpen, L. G.; Petrescu, S.; Birjega, R.; et al. Cellulose defibrillation and functionalization by plasma in liquid treatment. *Sci. Rep.* **2018**, *8*, 15473.
(38) Amaniampong, P. N.; Karam, A.; Trinh, Q. T.; Xu, K.; Hirao, H.; Jérôme, F.; Chatel, G. Selective and Catalyst-free Oxidation of D-Glucose to D-Glucuronic acid induced by High-Frequency Ultrasound. *Sci. Rep.* **2017**, *7*, 40650.
(39) Jin, B.; Yao, G.; Wang, X.; Ding, K.; Jin, F. Photocatalytic Oxidation of Glucose into Formate on Nano TiO2 Catalyst. *ACS Sustain. Chem. Eng.* **2017**, *5*, 6377−6381.
(40) Leitzen, S.; Vogel, M.; Steffens, M.; Zapf, T.; Müller, C. E.; Brandl, M. Quantification of Degradation Products Formed during Heat Sterilization of Glucose Solutions by LC-MS/MS: Impact of Autoclaving Temperature and Duration on Degradation. *Pharmaceuticals* **2021**, *14*, 1121.
(41) Yin, Y.; Ma, C.; Li, W.; Luo, S.; Liu, Y.; Wu, X.; Wu, Z.; Liu, S. Rapid conversion of glucose to 5-hydroxymethylfurfural using a MoCl3 catalyst in an ionic liquid with microwave irradiation. *Ind. Crops Prod.* **2021**, *160*, 113091.
(42) Tampieri, F.; Ginebra, M. P.; Canal, C. Quantification of Plasma-Produced Hydroxyl Radicals in Solution and their Dependence on the pH. *Anal. Chem.* **2021**, *93*, 3666−3670.
(43) Klose, S. J.; Ellis, J.; Riedel, F.; Schröter, S.; Niemi, K.; Semenov, I. L.; Weltmann, K. D.; Gans, T.; O'Connell, D.; van Helden, J. H. The spatial distribution of hydrogen and oxygen atoms in a cold atmospheric pressure plasma jet. *Plasma Sources Sci. Technol.* **2020**, *29*, 125018.
(44) Jablonowski, H.; Santos Sousa, J.; Weltmann, K. D.; Wende, K.; Reuter, S. Quantification of the ozone and singlet delta oxygen produced in gas and liquid phases by a non-thermal atmospheric plasma with relevance for medical treatment. *Sci. Rep.* **2018**, *8*, 12195.
(45) Wan, D.; Yang, H.; Yan, C.; Song, F.; Liu, Z.; Liu, S. Differentiation of glucose-containing disaccharides isomers by fragmentation of the deprotonated non-covalent dimers using negative electrospray ionization tandem mass spectrometry. *Talanta* **2013**, *115*, 870−875.
(46) Kailemia, M. J.; Ruhaak, L. R.; Lebrilla, C. B.; Amster, I. J. Oligosaccharide analysis by mass spectrometry: a review of recent developments. *Anal. Chem.* **2014**, *86*, 196−212.
(47) O'Sullivan, D. W.; Tyree, M. The kinetics of complex formation between Ti(IV) and hydrogen peroxide. *Int. J. Chem. Kinet.* **2007**, *39*, 457−461.
(48) Bekeschus, S.; Schmidt, A.; Niessner, F.; Gerling, T.; Weltmann, K. D.; Wende, K. Basic Research in Plasma Medicine—A Throughput Approach from Liquids to Cells. *J. Vis. Exp.* **2017**, *129*, 56331.
(49) Linxiang, L.; Abe, Y.; Nagasawa, Y.; Kudo, R.; Usui, N.; Imai, K.; Mashino, T.; Mochizuki, M.; Miyata, N. An HPLC assay of hydroxyl radicals by the hydroxylation reaction of terephthalic acid. *Biomed. Chromatogr.* **2004**, *18*, 470−474.
(50) Nasri, Z.; Bruno, G.; Bekeschus, S.; Weltmann, K.-D.; von Woedtke, T.; Wende, K. Development of an electrochemical sensor for in-situ monitoring of reactive species produced by cold physical plasma. *Sens. Actuators B Chem.* **2021**, *326*, 129007.
(51) Lackmann, J. W.; Bruno, G.; Jablonowski, H.; Kogelheide, F.; Offerhaus, B.; Held, J.; Schulz-von der Gathen, V.; Stapelmann, K.; von Woedtke, T.; Wende, K. Nitrosylation vs. oxidation—How to modulate cold physical plasmas for biological applications. *PLoS One* **2019**, *14*, No. e0216606.
(52) Jablonowski, H.; Santos Sousa, J.; Schmidt-Bleker, A.; Winter, J.; Wende, K.; von Woedtke, T.; Weltmann, K.-D.; Reuter, S. Plasma induced reactive oxygen species in biorelevant liquids: different species have various origins. *6th International Conference on Plasma Medicine (ICPM-6)*: Bratislava, Slovakia, September 4-9, 2016, 2016.
(53) Wende, K.; von Woedtke, T.; Weltmann, K. D.; Bekeschus, S. Chemistry and biochemistry of cold physical plasma derived reactive species in liquids. *Biol. Chem.* **2018**, *400*, 19−38.
(54) Sarangapani, C.; Ryan Keogh, D. R.; Dunne, J.; Bourke, P.; Cullen, P. J. Characterisation of cold plasma treated beef and dairy lipids using spectroscopic and chromatographic methods. *Food Chem.* **2017**, *235*, 324−333.
(55) Lackmann, J. W.; Wende, K.; Verlackt, C.; Golda, J.; Volzke, J.; Kogelheide, F.; Held, J.; Bekeschus, S.; Bogaerts, A.; Schulz-von der Gathen, V.; et al. Chemical fingerprints of cold physical plasmas—an experimental and computational study using cysteine as tracer compound. *Sci. Rep.* **2018**, *8*, 7736.
(56) Calvano, C. D.; Cataldi, T. R. I.; Kögel, J. F.; Monopoli, A.; Palmisano, F.; Sundermeyer, J. Structural Characterization of Neutral Saccharides by Negative Ion MALDI Mass Spectrometry Using a Superbasic Proton Sponge as Deprotonating Matrix. *J. Am. Soc. Mass Spectrom.* **2017**, *28*, 1666−1675.
(57) Von Seggern, C. E.; Cotter, R. J. Fragmentation studies of noncovalent sugar−sugar complexes by infrared atmospheric pressure MALDI. *J. Am. Soc. Mass Spectrom.* **2003**, *14*, 1158−1165.
(58) Delaux, J.; Ortiz Mellet, C.; Canaff, C.; Fourré, E.; Gaillard, C.; Barakat, A.; García Fernández, J. M.; Tatibouët, J.-M.; Jérôme, F. Impact of non-thermal atmospheric plasma on the structure of cellulose: access to soluble branched glucans. *Chem.—Eur. J.* **2016**, *22*, 16522−16530.
(59) Iglesias, J.; Martínez-Salazar, I.; Maireles-Torres, P.; Martin Alonso, D.; Mariscal, R.; López Granados, M. Advances in catalytic routes for the production of carboxylic acids from biomass: a step forward for sustainable polymers. *Chem. Soc. Rev.* **2020**, *49*, 5704−5771.
(60) Padovani, A. *Glucose Oxidation into Gluconic Acid*, 2017. https://hss-opus.ub.ruhr-uni-bochum.de/opus4/frontdoor/index/index/docId/5144.
(61) Lee, J.; Saha, B.; Vlachos, D. G. Pt catalysts for efficient aerobic oxidation of glucose to glucaric acid in water. *Green Chem.* **2016**, *18*, 3815−3822.
(62) Domon, B.; Costello, C. E. A systematic nomenclature for carbohydrate fragmentations in FAB-MS/MS spectra of glycoconjugates. *Glycoconj. J.* **1988**, *5*, 397−409.
(63) Schmidt-Bleker, A.; Winter, J.; Bösel, A.; Reuter, S.; Weltmann, K. D. On the plasma chemistry of a cold atmospheric argon plasma jet with shielding gas device. *Plasma Sources Sci. Technol.* **2016**, *25*, 015005.
(64) Tresp, H.; Hammer, M. U.; Weltmann, K.-D.; Reuter, S. Effects of Atmosphere Composition and Liquid Type on Plasma-Generated Reactive Species in Biologically Relevant Solutions. *Plasma Med.* **2013**, *3*, 45−55.
(65) Schuchmann, M. N.; Sonntag, C. v. Free Radical Induced Oxidation of Neutral Aqueous Solutions of D-Glucose in the Presence of Oxygen—a Non-Chain Process. *Z. Naturforsch. B* **1978**, *33*, 329−331.
(66) Bujak, P.; Bartczak, P.; Polanski, J. Highly efficient room-temperature oxidation of cyclohexene and d-glucose over nanogold Au/SiO2 in water. *J. Catal.* **2012**, *295*, 15−21.
(67) Moreno, T.; Kouzaki, G.; Sasaki, M.; Goto, M.; Cocero, M. J. Uncatalysed wet oxidation of d-glucose with hydrogen peroxide and its combination with hydrothermal electrolysis. *Carbohydr. Res.* **2012**, *349*, 33−38.
(68) Ghimire, B.; Szili, E. J.; Patenall, B. L.; Lamichhane, P.; Gaur, N.; Robson, A. J.; Trivedi, D.; Thet, N. T.; Jenkins, A. T. A.; Choi, E. H.; et al. Enhancement of hydrogen peroxide production from an atmospheric pressure argon plasma jet and implications to the antibacterial activity of plasma activated water. *Plasma Sources Sci. Technol.* **2021**, *30*, 035009.
(69) Attri, P.; Kim, Y. H.; Park, D. H.; Park, J. H.; Hong, Y. J.; Uhm, H. S.; Kim, K. N.; Fridman, A.; Choi, E. H. Generation mechanism of

https://doi.org/10.1021/acsomega.2c02965
ACS Omega 2022, 7, 31983−31998

hydroxyl radical species and its lifetime prediction during the plasma-initiated ultraviolet (UV) photolysis. *Sci. Rep.* **2015**, *5*, 9332.
(70) Tarr, M.; Paul Valenzeno, D. P. Singlet oxygen: the relevance of extracellular production mechanisms to oxidative stress in vivo. *Photochem. Photobiol. Sci.* **2003**, *2*, 355−361.
(71) Benedikt, J.; Mokhtar Hefny, M.; Shaw, A.; Buckley, B. R.; Iza, F.; Schäkermann, S.; Bandow, J. E. The fate of plasma-generated oxygen atoms in aqueous solutions: non-equilibrium atmospheric pressure plasmas as an efficient source of atomic O(aq). *Phys. Chem. Chem. Phys.* **2018**, *20*, 12037−12042.
(72) Matros, A.; Peshev, D.; Peukert, M.; Mock, H.-P.; Van den Ende, W. Sugars as hydroxyl radical scavengers: proof-of-concept by studying the fate of sucralose in Arabidopsis. *Plant J.* **2015**, *82*, 822−839.
(73) Rinsant, D.; Chatel, G.; Jérôme, F. Efficient and Selective Oxidation of D-Glucose into Gluconic acid under Low-Frequency Ultrasonic Irradiation. *Chemcatchem* **2014**, *6*, 3355−3359.
(74) Wende, K.; Williams, P.; Dalluge, J.; Van Gaens, W. V.; Aboubakr, H.; Bischof, J.; von Woedtke, T.; Goyal, S. M.; Weltmann, K. D.; Bogaerts, A.; et al. Identification of the biologically active liquid chemistry induced by a nonthermal atmospheric pressure plasma jet. *Biointerphases* **2015**, *10*, 029518.
(75) Omlid, S. M.; Dergunov, S. A.; Isor, A.; Sulkowski, K. L.; Petroff, J. T.; Pinkhassik, E.; McCulla, R. D. Evidence for diffusing atomic oxygen uncovered by separating reactants with a semi-permeable nanocapsule barrier. *Chem. Commun.* **2019**, *55*, 1706−1709.
(76) Hefny, M. M.; Pattyn, C.; Lukes, P.; Benedikt, J. Atmospheric plasma generates oxygen atoms as oxidizing species in aqueous solutions. *J. Phys. D: Appl. Phys.* **2016**, *49*, 404002.

https://doi.org/10.1021/acsomega.2c02965
ACS Omega 2022, 7, 31983−31998